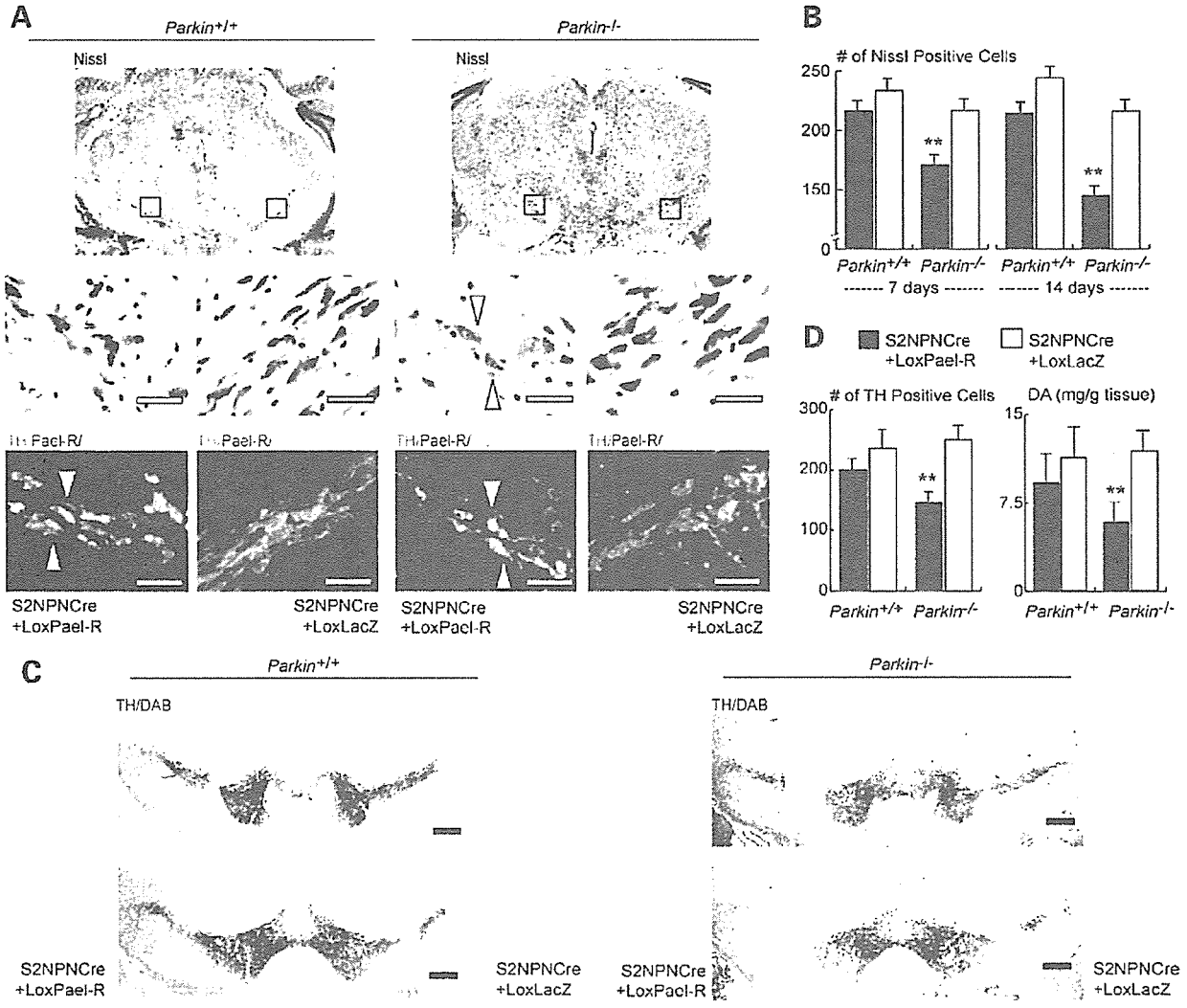

Figure 3. Enhanced neuronal death in the SNpc of parkin$^{-/-}$ mice by the up-regulation of Pael-R. (**A**) Adenoviral vectors (2 μl), including LoxEGFP (5×10^8 p.f.u.), S2NPNCre (10^9 p.f.u.) and LoxPael-R (10^9 p.f.u.) were injected unilaterally in the striatum of either parkin$^{+/+}$ or parkin$^{-/-}$ mice, as described in Figure 1. As a control, LoxPael-R was replaced by LoxLacZ (10^9 p.f.u.), and S2NPNCre + LoxLacZ was injected on the contralateral side. Brains of animals were then perfusion-fixed 7 days later, and midbrain sections were stained using the Nissl method (upper two panels). One of consecutive sections was also immunostained with anti-Pael-R antibody (lower panels). Images at −3.52 mM from the Bregma are shown. The open boxes in the upper panel are magnified in lower two panels. Typical examples of neurons positive with both TH and Pael-R are indicated by white arrowheads in the lower panels. Typical examples of degenerating neurons are identified by the open arrowheads in the middle panels. (**B**) Nissl positive neurons were counted on the ipsilateral (closed bars) and contralateral sides (open bars) as described in the text, 7 and 14 days after the injection. In each case, $n = 6$, and the mean ± SD is shown. ** denotes $P < 0.01$ compared to parkin$^{+/+}$ mice injected with LoxLacZ. (**C**) 10 days after the injection, midbrain sections were stained with anti-TH antibody as described in text. Images at −3.28 mM (upper panels) and −3.52 mM from the Bregma (lower panels) are shown. (**D**) TH positive neurons were counted 7 days after the injection (left panel). DA content was also measured by the HPLC-EC method 7 days after the injection (right panel). In each case, closed and open bars correspond to the ipsilateral (closed bars) or contralateral striatum (open bars) of parkin$^{-/-}$ or parkin$^{+/+}$ mice, respectively. In each case, $n = 6$, and the mean ± SD is shown. ** denotes $P < 0.01$ compared to parkin$^{+/+}$ mice injected with LoxLacZ.

side received injection of S2NPNCre, LoxPael-R and LoxEGFP) based on EGFP fluorescence or Nissl staining (Supplementary Material, Fig. S2B), diminished dopamine content most likely reflects loss of functional dopaminergic neurons in the ipsilateral SNpc. Moreover, injection of S2NPNCre and LoxPael-R resulted in the expression of Pael-R (marked by expression of EGFP) also in the motor cortex by retrograde infection (Supplementary Material, Fig. S2A). In contrast to the SNpc, no neuronal death was observed in either motor cortex or striatum (Supplementary Material, Fig. S2C). In other brain sublesions which have the connection to the striatum (i.e. the thalamus, the interpeduncular nucleus, the locus coeruleus and the raphe nucleus), no EGFP signals were detected, which may be due to the fewer communication to the striatum (not shown). The loss of TH immunointensity in the SNpc mainly occurred in neurons expressing Pael-R (Supplementary Material, Fig. S3A–C). These data suggest that Pael-R overexpression caused neuronal cell death, rather selectively in dopaminergic neurons in the SNpc.

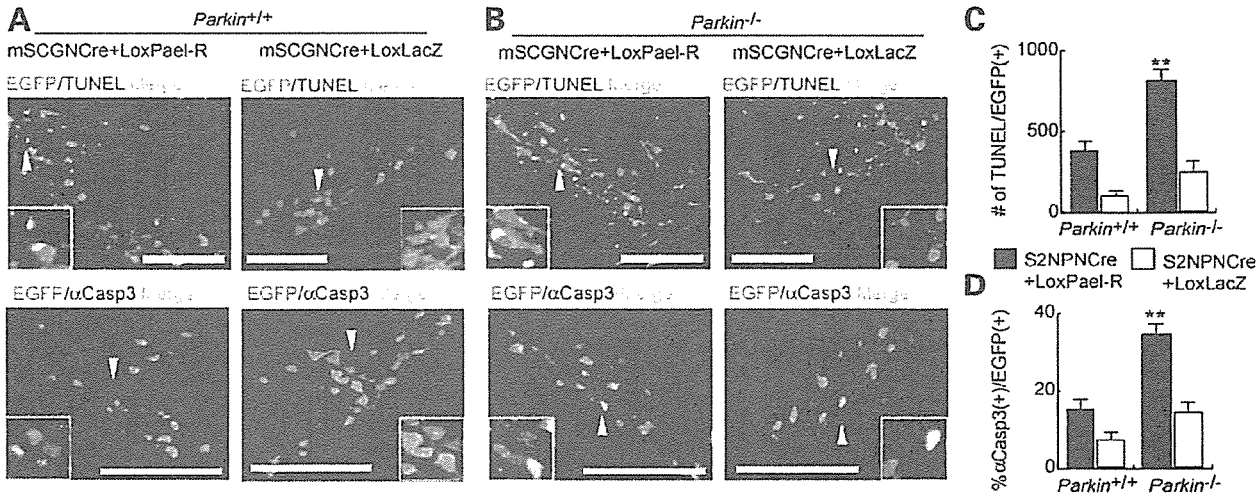

Figure 4. Assessment of neuronal cell death in parkin$^{-/-}$ mice (**A,B**) After infection of adenoviral vectors by the same protocol as used in Figure 3, brains of animals were perfusion-fixed 7 (upper panels for TUNEL) and 5 (lower panels for activated caspase-3 staining) days later, and midbrain sections were stained using either the TUNEL method or anti-activated caspase-3 antibody (αCasp3). Images at −3.52 mM from the Bregma were obtained to visualize the indicated antibody and the EGFP signal (green). In each panel, areas indicated by arrowheads are magnified in the insets at the lower corner of the panel. Note that TUNEL-positive and activated caspase-3-positive cells are increased in the EGFP positive area. Scale bar: 200 μm. Images shown in this figure (panels A,B) are representative of six repeated experiments. (**C,D**) Quantitation of TUNEL-positive signals (number of positive signals) 7 days after injection (panel C) or the percentage of cells positive for activated caspase-3 (αCasp3) in the population of EGFP-positive neurons 5 days after injection (panel D) on the ipsilateral (closed bars) or contralateral SNpc (open bars) of either parkin$^{-/-}$ or parkin$^{+/+}$ mice. In each case, $n = 6$, and the mean ± SD is shown. ** denotes $P < 0.01$ compared to parkin$^{+/+}$ mice injected with LoxLacZ.

ORP150 suppresses Pael-R-mediated neuronal cell death

These observations led us to hypothesize that ER stress might trigger loss of dopaminergic neurons due to accumulation of toxic Pael-R. To gain further insight into mechanisms underlying this observation, we focused on the function of an ER chaperone, ORP150, which promotes protein folding/degradation (17). We reasoned that if the ER stress is the cause of Pael-R-mediated dopaminergic neuron death, even in the presence of wild-type *Parkin*, decreased levels of ORP150 should accentuate Pael-R-induced neuronal death in the SNpc, whereas overexpression of ORP150 might be protective. Using targeted injection of adenoviral vectors (as above), Pael-R was overexpressed in the SNpc of either heterozygous *Orp150* truncation mutants [*Orp150*$^{+/-}$ mice; note, homozygous *Orp150*$^{-/-}$ mice have a developmental lethal phenotype 13)], strain-matched controls (*Orp150*$^{+/+}$ mice) or *Orp150* overexpressing wild-type transgenics [*Orp150* TG mice, driven by pCAGGS promoter (21)]. Elevated levels of ORP150 were confirmed in SNpc neurons of *Orp150* TG mice by immunohistochemical analysis (Supplementary Material, Fig. S4 upper panels; levels of ORP150 in strain-matched normal animals are also shown in lower panels). Degeneration of dopaminergic neurons was assessed by TUNEL staining and expression of activated caspase-3 (Fig. 5A and B), since these methods appeared to have adequate sensitivity, as shown in Figure 4. A gene dosage effect was observed; increased levels of ORP150 afforded protection to dopaminergic neurons. *Orp150*$^{+/-}$ mice, with the lowest levels of functional ORP150, displayed exaggerated damage to dopaminergic neurons; TUNEL staining and activated caspase-3 were enhanced on the ipsilateral SNpc (the side in which injection of adenoviral vectors resulted in over-expression of Pael-R; Fig. 5A and B), whereas no significant cell death was observed on the contralateral side where LoxLacZ was expressed (data not shown). Each of these indices of neuronal stress/toxicity in this setting was decreased, in a manner dependent on the 'dose' of *Orp150*, when the same experiment was performed in wild-type (*Orp150*$^{+/+}$) or mice overexpressing ORP150 (*Orp150* TG mice) (Fig. 5A and B).

These data suggest an essential contribution of ER function in protecting neurons from lethal toxicity when Pael-R is overexpressed. According to this concept, we further reasoned that such neurons in *Parkin*$^{-/-}$ mice might be rescued by either expression of Parkin or ER chaperones capable of promoting protein folding/renaturation, such as GRP78. Though adenoviral expression of LacZ in neurons failed to rescue SNpc neurons from Pael-R-mediated cell death, overexpression of Parkin minimized neuronal damage (Fig. 5C). Similarly, overexpression of GRP78 could substitute for Parkin in preventing Pael-R-mediated neuronal death in *Parkin*$^{-/-}$ mice. Western blot analysis of brain stem samples confirmed the expression of transfected gene products (Fig. 5C, right panel). These data indicate that the ER chaperones, such as GRP78 and ORP150, have the capacity to relieve ER stress due to increased expression of Pael-R, thereby exerting a protective effect on dopaminergic neurons in the SNpc.

Suppression of Pael-R-mediated cell death by inhibition of dopamine synthesis

Increased dopamine content in the striatum of *Parkin*$^{-/-}$ mice has been noted by some investigators, though the increase is small (18,19). Furthermore, Pael-R has been implicated in

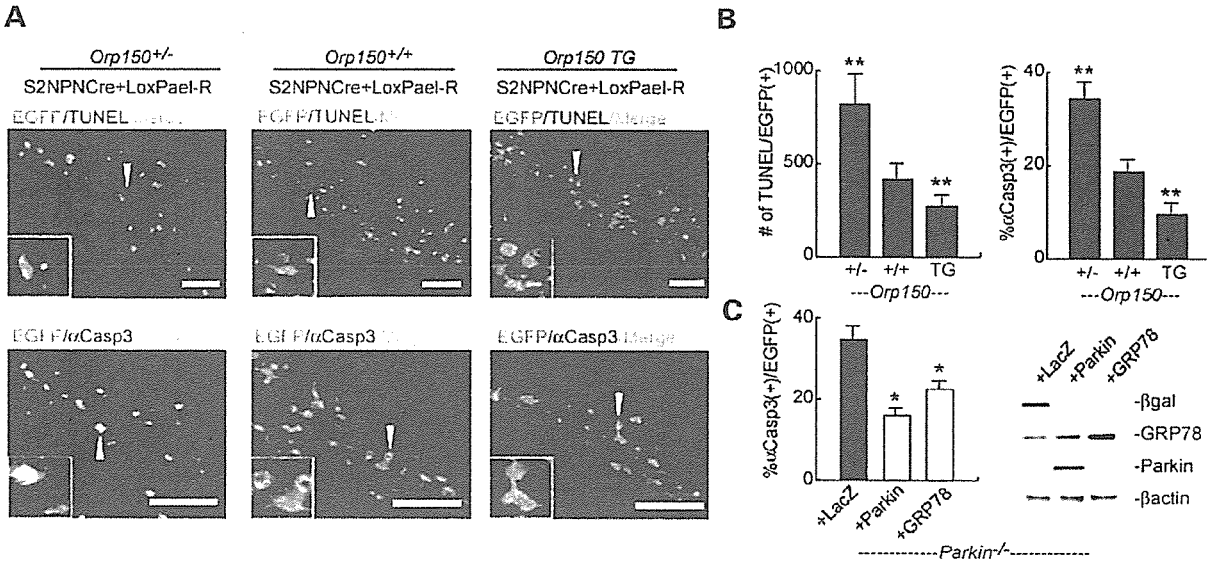

Figure 5. Effect of ORP150, Parkin, and GRP78 on Pael-R-mediated cell death in the SNpc. (**A**) Adenoviral vectors (2 μl), including LoxEGFP (5×10^8 p.f.u.), S2NPNCre (10^9 p.f.u.), and LoxPael-R (10^9 p.f.u.), were injected unilaterally into the striatum of either ORP150$^{+/-}$ (left panels), ORP150$^{+/+}$ (middle panels) or ORP150 transgenic mice (ORP150 TG; right panels) mice. Where indicated, LoxPael-R was replaced with LoxLacZ (10^9 p.f.u.), and the latter mixture was injected on the contralateral side. Brains were then perfusion fixed at 7 (for TUNEL analysis; upper panels) and 5 (for activated caspase-3 staining; αCasp3, lower panels) days after the injection. Images were overlapped with the EGFP signal (green). In each panel, the area indicated by the arrowhead is magnified in a small inset in the lower corner. Note the increase in cells staining positively by TUNEL analysis and for activated caspase-3 antigen in the EGFP positive area. This was most apparent in ORP150$^{+/-}$ mice. Scale bar: 200 μm. All images shown in this figure are representative of six repeated experiments. (**B**) Total number of TUNEL-positive signals (left panel) and the percentage of activated caspase-3 (αCasp3) positive cells in the population of EGFP-positive neurons (right panels) determined in the ipsilateral SNpc. In each case, $n = 6$, and the mean ± SD is shown. ** denotes $P < 0.01$ compared to ORP150$^{+/+}$ (wild type) mice. (**C**) A mixture (total 2 μl) of LoxEGFP (5×10^8 p.f.u.), S2NPNCre (10^9 p.f.u.), LoxPael-R (10^9 p.f.u.), and LoxLacZ (1.5×10^9 p.f.u.) was injected unilaterally into the striatum of parkin$^{-/-}$ mice. On the contralateral side, LoxLacZ was replaced with either AxCMParkin (Parkin; 1.5×10^9 p.f.u.) or AxCAGRP78 (GRP78; 1.5×10^9 p.f.u.). Midbrain sections were stained with anti-activated caspase-3 antibody (5 days later). The percentage of activated caspase-3-positive neurons was determined on the ipsilateral (closed bars) and contralateral sides. In the latter case, data is shown following injection of the vector expressing parkin (gray bars) and GRP78 (open bars) are shown. In each case, $n = 6$, and the mean ± S.D is shown. Midbrain samples collected from parkin$^{-/-}$ mice as described in text were also subjected to Western blot analysis using either anti-β-galactosidase, anti-GRP78, anti-Parkin or anti-β-actin antibody (for an internal control). A typical example of five repeated experiments is shown. * denotes $P < 0.01$ compared to the group injected with the vector expressing LacZ.

the regulation of dopamine levels; increased Pael-R is associated with increased dopamine content in the striatum (Imai, Y. *et al.*, manuscript in preparation). Based on these observations, we reasoned that Pael-R-mediated cell death in the SNpc of *Parkin*$^{-/-}$ mice might be associated with elevated levels of dopamine. Since dopamine has considerable potential toxicity (8,22), we further hypothesized that dopamine-derived metabolites/catabolites might contribute to loss of TH-positive (+) neurons. To address this issue directly, we determined whether suppression of DA synthesis by AMPT, a specific inhibitor of TH (15), would have a neuroprotective effect on TH(+) neurons overexpressing Pael-R in the SNpc of *Parkin*$^{-/-}$ mice. Accidental death of mice occurred in ≈4% of animals within 36 h after the first administration of AMPT. This might be due to the shifts of circadian temperature rhythms (23). The systemic toxicity of AMPT was not observed at later phase. Repeated administration of AMPT over a 7 day period lowered dopamine content of the striatum to ≈30% of that observed in untreated controls (Supplementary Material, Fig. S5). Using this protocol of AMPT treatment, adenoviral vectors were injected into the striatum to increase neuronal Pael-R levels in *Parkin*$^{-/-}$ mice. Compared with *Parkin*$^{-/-}$ mice treated with phosphate-buffered saline (PBS), animals receiving AMPT displayed striking neuroprotection. Inhibition of TH in *Parkin*$^{-/-}$ mice overexpressing Pael-R in the SNpc suppressed the number of TUNEL-positive nuclei and generation of activated caspase-3 epitopes, compared with animals treated with PBS alone (Fig. 6A–C). AMPT treatment was also effective in preventing Pael-R-mediated cell death in the SNpc of *Orp150*$^{+/-}$ mice, compared with animals treated with saline (Fig. 6C), suggesting a toxic effect of DA in ER dysfunction. These data suggest that dopamine enhances neurotoxicity associated with overexpression of Pael-R, especially in the absence of Parkin.

DISCUSSION

Our data indicate that *in vivo* overexpression of Pael-R in neurons of the SNpc results in enhanced ER stress, which, especially in a setting with decreased functional Parkin, targets TH-positive neurons for accentuated cytotoxicity. Whereas expression of a protein as difficult to properly fold as Pael-R has been shown to cause ER stress in a range of cell types *in vitro* (9), we believe that cellular vulnerability in this situation is critically exaggerated in dopaminergic neurons *in vivo* due to the superimposed toxicity of dopamine

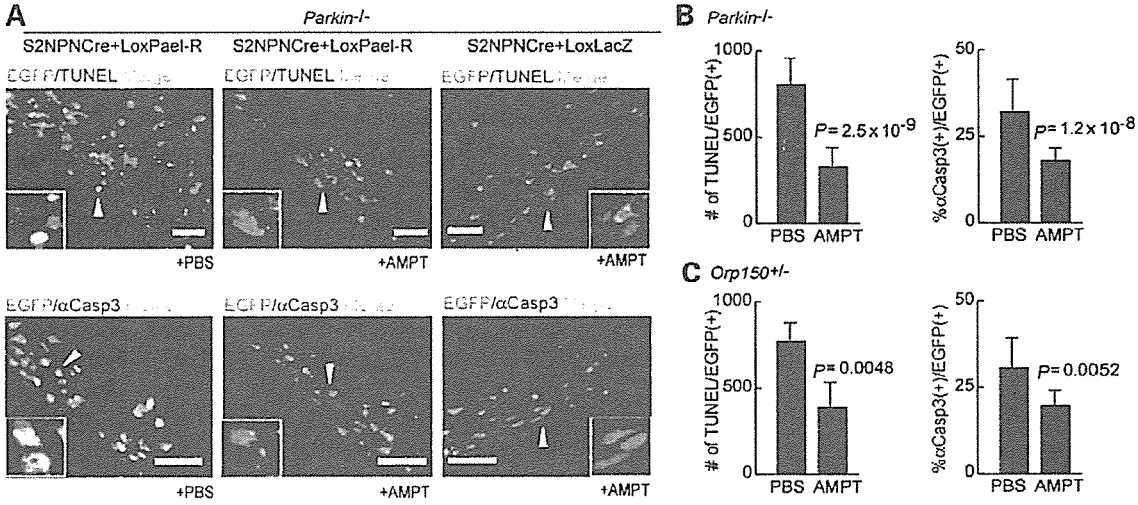

Figure 6. Suppression of neuronal death in the SNpc of mice overexpressing Pael-R by inhibition of dopamine synthetase using AMPT. (**A**) Parkin$^{-/-}$ mice were treated with either PBS or AMPT up to 7 days after unilateral injection of adenoviral vectors, including LoxEGFP (5×10^8 p.f.u.), S2NPNCre (10^9 p.f.u.) and LoxPael-R (10^9 p.f.u.). As a control, the same vectors, with LoxPael-R replaced by LoxLacZ (10^9 p.f.u.), were injected on the contralateral side. Brains were perfusion-fixed at 7 (upper panels; for TUNEL analysis) and 5 (lower panels; staining for activated caspase-3, αCasp3) days after injection of the vectors, and were then subjected to histochemical analysis as described above. The above images were overlapped with EGFP (green). Scale bar: 200 μm. All images shown in this figure are representative of six repetitions of the experimental protocol. In each panel, the area indicated by the arrowhead is magnified in a small inset in the lower corner. Note that TUNEL-positive and activated caspase-3-positive cells were diminished by AMPT treatment (i.e. in the presence of the latter, the area/level of apoptotic cells approximated that observed in controls overexpressing LacZ). (**B,C**) Statistical analysis was performed as described above, in either *Parkin*$^{-/-}$ mice (B) or *Orp150*$^{+/-}$ mice (C). The number of TUNEL-positive signals (left panels), and % of activated caspase-3-positive cells in the population of EGFP-positive neurons (right panels) in the ipsilateral SNpc are shown ($n = 6$; the mean ± SD). *P*-values obtained by Student's t-analysis, are shown in each panel.

(DA) itself. These data also emphasize the potential relevance of parkin targets, such as Pael-R, in addition to the aminoacyl-tRNA synthetase cofactor p38, to neurotoxicity in dopaminergic neurons (24).

The technical approach employed in our experiments, injection of adenovirus under stereotactic guidance into the striatum with selective neuronal expression of gene products, is quite unique. First, such results have been difficult to achieve in the mouse because of anatomic limitations. Though adenovirus vectors are more immunogenic than adenovirus associated virus, they still have greater merits in retrograde transfection (25). We have taken this advantage into our experimental system, to achieve an efficient gene transfer to SNpc, where direct injection of viral vectors will be inapplicable because of anatomical limitations. Second, adenovirus infection predominately affects glia, rather than neurons. Modification of the SCG10 (superior cervical ganglion) promoter by tandem insertion of two neuron-restrictive silencers produced almost 100% expression of transgenes in neuronal cultures, and considerably lower expression in astrocytes (not shown). Coinjection of S2NPNCre with LoxEGFP into the striatum resulted in expression of transgenes in neurons of the mouse SNpc. This approach allowed us to obtain neuron-specific expression of Pael-R enabling study of its effect(s) on neuronal physiology *in vivo*. The proximal result of such Pael-R expression included upregulation of ER chaperones, such as GRP78 and ORP150, whereas the distal result was loss of TH-positive neurons, especially in *Parkin*$^{-/-}$ mice. In contrast, expression of Pael-R had no effect on the constitutively expressed form of HSP70, important for housekeeping functions in the cytoplasm (Fig. 2D).

Several observations are consistent with the importance of ER stress as a mechanism underlying Pael-R-induced cellular toxicity. In previous studies using cultured neuroblastoma cells, Pael-R has been identified as a substrate of Parkin, an E3 ubiquitin ligase (6). Thus, in the absence of Parkin, Pael-R may accumulate since it is not subject to efficient removal. In contrast, no detectable change of Pael-R levels has been reported in SNpc of Parkin null mice (24). Since there is no evidence of progressive neuronal cell death in Parkin null mice, there would appear to be redundant mechanisms able to compensate for loss of Parkin under physiologic conditions. The ability of neurons to withstand ER stress imposed by expression of Pael-R is likely to be dependent on the effectiveness of the ER-stress response; higher levels of Pael-R would require a facile ER-stress response (i.e. adequate or increased levels of parkin, ORP150, GRP78 etc), whereas diminished levels of ORP150 or GRP78 would render neurons vulnerable to toxicity because of a compromised stress response. These predictions have been borne out by our experimental results. Therefore, the possible toxicity of Pael-R cannot be completely ignored, especially in pathological conditions. Increasing expression of GRP78 had a protective effect in *Parkin*$^{-/-}$ mice overexpressing Pael-R. Furthermore, expression of ORP150, an important factor modulating ER stress even in the presence of Parkin, modulated the toxicity of Pael-R for dopaminergic neurons; increased levels of ORP150 in transgenic mice were neuroprotective, whereas diminished levels of ORP150 in *Orp150*$^{+/-}$ mice resulted in enhanced cell death (i.e. increased TUNEL staining and immunoreactivity for activated caspase-3 in the SNpc).

Our experimental system produced Pael-R overexpression and subsequent cell death in the SNpc of mouse, whereas no apparent cell death occurred either in the striatum or in the motor cortex (Supplementary Material, Fig. S2C). Furthermore, we observed a neuroprotective effect of a TH inhibitor in the SNpc of mouse, suggesting that DA also contributes to Pael-R-induced cell death of dopaminergic neurons. Consistent with these results in our mouse models, studies in transgenic flies overexpressing Pael-R in most of neuronal populations also showed selective loss of dopaminergic neurons, though the mechanism of cellular degeneration is not fully understood (10). One plausible explanation for focusing toxicity on dopaminergic neurons is the oxidative stress caused by the presence of DA and its derivatives (1). Another possibility that DA might compromise the survival of dopaminergic neurons is a chemical inactivation of cellular proteins by addition of DA to sulfhydryl group of proteins. Recently, it has been reported that dopamine covalently modifies Parkin, a protein rich in sulfhydryl group, in dopaminergic cells, leading to increased Parkin insolubility and inactivation of its E3 function (22). Vulnerability of Parkin to modification by DA further impairs degradation of Pael-R. Thus, even in sporadic PD, DA might interfere in the degradation of certain proteins, such as Pael-R, by the inactivation of Parkin. Collectively, these data propose a model in which a combination of ER stress and DA-related stress plays an important role in degeneration of dopaminergic neurons in sporadic PD as well as PD caused by *parkin* mutations.

MATERIALS AND METHODS

Targeted disruption of the mouse parkin gene

Parkin$^{-/-}$ mice were generated using standard gene targeting techniques (26). A targeting vector was constructed with a 15.7 kb genomic DNA fragment containing exon 3 of the parkin gene (Supplementary Material, Fig. S1). The region containing exon 3 was replaced with a Floxed pgk-neo cassette. A DT-ApA cassette was flanked at the 5′-end of the homologous arm for negative selection (27). The linearized targeting vector was transfected into E14 (129sv) ES cells. Positive clones were selected by Southern blotting, and then injected into C57Bl/6J (B6) blastocysts. Offspring harboring the targeted allele were generated by crossing chimeric mice with B6 mice. Results of such crosses were confirmed by Southern analysis.

Reverse transcription–polymerase chain reaction analysis of parkin null mice

Total RNA was extracted from whole brain tissue using Isogen (Nippon gene). RT reactions containing 1 μg of total RNA were performed using the SuperScript II First-Strand Synthesis System for RT–PCR (Invitrogen). The resulting cDNA was added to PCR reactions containing 1 unit of Ex *Taq* DNA Polymerase (Takara) for 35 PCR cycles. PCR products were separated on a 1% agarose gel. Primers were as follows: RT primer, 5′-agt ttc cct tga ggt tgt gc; Primer A, 5′-cgt agg tcc ttc tcg acc; Primer B, 5′-ttg agg ttg tgc gtc cag g; Primer C, 5′-acc tca gag ggc tcc ata tg; and, Primer D, 5′-ctc tct cta cac gtc aaa cca gtg.

Construction of adenoviral vectors

Modified SCG10 (S2NP10) promoter [2 kb (28)] and mouse GFAP promoter region (2.5 kb; kindly provided by Dr Ikenaka, National Institute for Physiological Science) were cloned into pAxAwNCre (kindly provided by Dr Saito, Tokyo University), a promoter-less cosmid vector for preparing cell type-specific Cre-recombinase expressing adenovirus (Fig. 2A; AxS2NPNCre and AxGFAPNCre). Human Pael-R (9) was cloned into pAxCALNLw (Takara Bio Inc., Shiga, Japan) in order to control Pael-R expression using Cre recombinase (AxLNLPael-R). The Pael-R gene is silenced because of the presence of the staffer of the neo-resistant gene, and is activated by Cre-mediated excisional deletion of the stuffer when a sufficient amount of Cre recombinase is expressed (Fig. 3). To prepare an adenoviral vector of parkin (AxCMParkin), the human parkin gene was cloned into pAxCMwt. Recombinant adenovirus was generating using the COS-terminal protein complex (TPC) method and the Takara adenovirus expression kit (Takara Bio Inc.). AxLNLNZ (Takara Bio Inc.), which overexpresses LacZ with a nuclear localization signal mediated by Cre recombinase, was used for control experiments. Cre-mediated EGFP-expressing adenovirus, AxLNLEGFP, was kindly provided by Dr Okado (Tokyo Metropolitan Institute of Neuroscience). An adenoviral vector for overexpression of GRP78/Bip (AxCAGRP78) was generously provided by Drs S. Tanaka and T. Koike [(29) Graduate School of Science, Hokkaido University]. Each adenovirus was amplified in HEK293 cells and purified using VIRAPREP Adenovirus Purification Kit (Virapur LLC., San Diego, CA, USA). Viral titers were determined by a plaque-forming assay in HEK293 cells.

Western blotting

Levels of Pael-R in tissue extracts were determined by Western blotting as described (9). Mouse brain was quickly removed and placed on a cold plate. Brain slices (200 μm) were obtained at −3.5 mM from the Bregma on a vibratome. Substantia nigra was then carefully removed under guidance of a stereoscopic microscope according to the mouse brain atlas (Paxinos and Franklin, Academic Press, 1997, San Diego) using the cerebral peduncle and medial lemniscus as landmarks. Tissue extracts were prepared from SNpc in PBS containing NP-40 (1%). Proteins were separated by SDS-PAGE, and transferred to PVDF. PVDF was then incubated with antibody to either human Pael-R or ß-actin, the latter as an internal control (1000 × dilution, Sigma, St Louis, MO, USA). Levels of chaperones in tissue extracts were determined by Western blotting, as described (30). PVDF was incubated with either anti-human ORP150 antibody (1 μg/ml), anti-GRP78 monoclonal antibody (Stressgen, Canada; 0.2 μg/ml), or anti-HSP73 antibody (0.1 μg/ml; Stressgen). Where indicated, either anti-β-galactosideas antibody (1000 × dilution, Sigma) or anti-Parkin antibody (1000 × dilution, Cell Signaling Technologies Inc.) was

used to access the level of these proteins. Images were further subjected to densitometric analysis using NIH image software.

Injection of adenoviral vectors into the striatum and treatment of animals

Animals were housed and treated according to institutional and national guidelines. Mice were stereotactically positioned under deep anesthesia, and the indicated combination of adenovirus vectors was injected unilaterally (a different combination, including a LacZ control, was injected on the contralateral side) into the striatum at six points (AP/ML/DV/ = 0.8/1.2/−2.5, 0.8/1.2/−3.2, 0.8/1.7/−2.5, 0.8/1.7/−3.2, 0.8/2.2/−2.5 and 0.8/2.2/−3.2; units are mm), followed by free access to food and water. Retrograde passage and infection of adenoviruses was confirmed 5–12 days after the injection by detection of a green fluorescent signal in the SNpc by fluorescence microscopy. Where indicated, animals were pretreated with α-methyl-DL-Tyrosine (AMPT) to suppress DA synthesis. AMPT-HCl (150 mg/kg, Sigma) was intra-peritoneally administrated twice per day for 5 days before injection of adenoviral vectors, as well as after the latter and until the day of sacrifice.

Assessment of neuronal death *in vivo*

At the indicated time points, animals were perfused with 4% paraformaldehyde under deep anesthesia, the brain was excised and coronal brain sections (14 μm) were cut on a cryostat. Sections were processed for cresyl violet staining or immunohistochemistry using either mouse anti-tyrosine hydroxylase antibody (TH; 1 μg/ml, Sigma), rabbit anti-human ORP 150 antibody [5 μg/ml (30)], rabbit anti-activated casepase-3 antibody(0.1 μg/ml, Genzyme/Teche), rabbit anti-Pael-R antibody [10 μg/ml, (9)] or goat anti-GFAP antibody (4 μg/ml. Santa Cruz Biotechnology, Santa Cruz, CA). Sections were also subjected to TUNEL staining using a commercially available kit (ApopTag, Intergen, Purchase, NY). To evaluate neuronal death in the SNpc, either Nissl or EGFP positive cells were counted in each coronal slice obtained at five different levels (−3.16, −3.28, −3.40, −3.52 and −3.64 mM from the Bregma), as described (31) by acquiring digital images using a CCD camera (Nikon, Coolscope). Cell death was semi-quantitatively assessed by counting TUNEL-positive cells/nuclei in the EGFP-positive area, and evaluating the percentage of activated caspase-3-positive cells in the population of EGFP-positive cells. Sections were analyzed using a laser scanning confocal microscope system (Leica, TCS SP2). In each case, two observers without knowledge of the experimental protocol evaluated sections and experiments were repeated at least three times.

DA content in the striatum was measured in the SNpc as described (32). In brief, striatal tissue was homogenized in solution H (0.4 M $HClO_4$ containing 4 mM $Na_2S_2O_5$, 4 mM diethylenetriaminepentaacetic acid, and 5 mM 1,4-dithiothreitol). Crude tissue lysate was separated on a C-18 reversed-phase column (MCM HPLC, 4.6 mM × 15 cm, 5 ml, ESA, Chelmsford, MA, USA), followed by electrochemical detection (Coulochem III, ESA).

Statistical analysis

Data shown represent the mean ± SD Multiple group comparisons were performed by one-way ANOVA, followed by Newman-Kuels test as a *post hoc* analysis. Comparison between two groups was analyzed by two-tailed Student's *t*-test.

SUPPLEMENTARY MATERIAL

Supplementary Material is available at HMG Online.

ACKNOWLEDGEMENTS

We thank Dr Martin Hooper (Western General Hospital, Edinburgh) for generous contribution of E14 cell line, and Drs Yumi Onodera, Yoshikazu Saito, Hitomi Suzuki (RIKEN, Wako, Japan) for technical assistance for establishing chimera mice. The authors also appreciate the generous gifts of AxCALNLEGFP, GAG promoter and Ax1CAGRP78 from Drs Haruo Okado (Tokyo Metropolitan Institute for Neuroscience), Jun-Ichi Miyazaki (Osaka University Medical School), and Shuuitsu Tanaka and Tetsuro Koike (Hokkaido University), respectively. This work was partially supported by the Ministry of Education, Science, Sports and Culture, a Grant-in-Aid for Scientific Research on Priority Areas—Advanced Brain Science Project—#15016120 to R.T., for Scientific Research (A) #14207032 to R.T., and for Young Scientists (A) #15680011 to Y.I. and a grant from the Special Postdoctoral Researcher Program of RIKEN to Y.I.

Conflict of Interest statement. None declared.

REFERENCES

1. Blum, D., Torch, S., Lambeng, N., Nissou, M., Benabid, A.L., Sadoul, R. and Verna, J.M. (1999) Molecular pathways involved in the neurotoxicity of 6-OHDA, dopamine and MPTP: contribution to the apoptotic theory in Parkinson's disease. *Trends. Biochem. Sci.*, **24**, 135–172.
2. Kitada, T., Asakawa, S., Hattori, N., Matsumine, H., Yamamura, Y., Minoshima, S., Yokochi, M., Mizuno, Y. and Shimizu, N. (1998) Mutations in the parkin gene cause autosomal recessive juvenile parkinsonism. *Nature*, **392**, 605–608.
3. Morett, E. and Bork, P. (1999) A novel transactivation domain in parkin. *Trends. Biochem. Sci.*, **24**, 229–231.
4. Jackson, P.K., Eldridge, A.G., Freed, E., Furstenthal, L., Hsu, J.Y., Kaiser, B.K. and Reimann, J.D. (2000) The lore of the RINGs: substrate recognition and catalysis by ubiquitin ligases. *Trends. Cell. Biol.*, **10**, 429–439.
5. Takahashi, R., Imai, Y., Hattori, N. and Mizuno, Y. (2003) Parkin and endoplasmic reticulum stress. *Ann. N.Y. Acad. Sci.*, **991**, 101–106.
6. Imai, Y., Soda, M. and Takahashi, R. (2000) Parkin suppresses unfolded protein stress-induced cell death through its E3 ubiquitin-protein ligase activity. *J. Biol. Chem.*, **275**, 35661–36664.
7. Shimura, H., Hattori, N., Kubo, S., Mizuno, Y., Asakawa, S., Minoshima, S., Shimizu, N., Iwai, K., Chiba, T., Tanaka, K. and Suzuki, T. (2000) Familial Parkinson disease gene product, parkin, is a ubiquitin-protein ligase. *Nat. Genet.*, **25**, 302–305.
8. Tanaka, K., Suzuki, T., Hattori, N. and Mizuno, Y. (2004) Ubiquitin, proteasome and parkin. *Biochim. Biophys. Acta.*, **29**, 235–247.
9. Imai, Y., Soda, M., Inoue, H., Hattori, N., Mizuno, Y. and Takahashi, R. (2001) An unfolded putative transmembrane polypeptide, which can lead to endoplasmic reticulum stress, is a substrate of Parkin. *Cell.*, **105**, 891–902.

10. Yang, Y., Nishimura, I., Imai, Y., Takahashi, R. and Lu, B. (2003) Parkin suppresses dopaminergic neuron-selective neurotoxicity induced by Pael-R in drosophila. *Neuron*, **27**, 911–924.
11. Tamatani, M., Matsuyama, T., Yamaguchi, A., Mitsuda, N., Tsukamoto, Y., Taniguchi, T., Che, Y.H., Ozawa, K., Hori, O., Nishimura, H. *et al.* (2001) ORP150 protects against hypoxia/ischemia-induced neuronal death. *Nat. Med.*, **7**, 317–323.
12. Miyazaki, M., Ozawa, K., Hori, O., Kitao, Y., Matsushita, K., Ogawa, S. and Matsuyama, T. (2002) Expression of ORP150 (150 kDa oxygen regulated protein) in the hippocampus suppresses delayed neuronal cell death. *J. Cereb. Blood Flow Metab.*, **22**, 979–987.
13. Kitao, Y., Ozawa, K., Miyazaki, M., Tamatani, M., Kobayashi, T., Yanagi, H., Okabe, M., Ikawa, M., Yamashima, T., Tohyama, M. *et al.* (2001) Expression of 150 kDa Oxygen Regulated Protein (ORP150), a molecular chaperone in the endoplasmic reticulum, rescues hippocampal neurons from glutamate toxicity. *J. Clin. Invest.*, **108**, 1439–1450.
14. Kitao, Y., Hashimoto, K., Matsuyama, T., Iso, H., Tamatani, T., Hori, O., Stern, D.M., Kano, M., Ozawa, K. and Ogawa, S. (2004) ORP150/HSP12A regulates Purkinje cell survival: a role for endoplasmic reticulum stress in cerebellar development. *J Neurosci.*, **24**, 1486–1496.
15. Dong, Z., Ferger, B., Paterna, J.C., Vogel, D., Furler, S., Osinde, M., Feldon, J. and Bueler, H. (2003) Dopamine-dependent neurodegeneration in rats induced by viral vector-mediated overexpression of the parkin target protein, CDCrel-1. *Proc. Natl Acad. Sci. U.S.A.*, **100**, 12438–12443.
16. Kanegae, Y., Lee, G., Sato, Y., Tanaka, M., Nakai, M., Sakaki, T., Sugano, S. and Saito, I. (1995) Efficient gene activation in mammalian cells by using recombinant adenovirus expressing site-specific Cre recombinase. *Nucleic Acids Res.*, **23**, 3816–3821.
17. Bando, Y., Ogawa, S., Yamaguchi, A., Kuwabara, K., Ozawa, K., Hori, O., Yanagi, H., Tamatani, M. and Tohyama, M. (2000) The 150 kDa Oxygen Regulated Protein (ORP150) functions as a novel molecular chaperone in the protein transport of the MDCK cells. *Am. J. Physiol. (Cell Physiol.)*, **278**, C1172–C1182.
18. Itier, J.M., Ibanez, P., Mena, M.A., Abbas, N., Cohen-Salmon, C., Bohme, G.A., Laville, M., Pratt, J., Corti, O., Pradier, L. *et al.* (2003) Parkin gene inactivation alters behaviour and dopamine neurotransmission in the mouse. *Hum. Mol. Genet*, **12**, 2277–2291.
19. Goldberg, M.S., Fleming, S.M., Palacino, J.J., Cepeda, C., Lam, H.A., Bhatnagar, A., Meloni, E.G., Wu, N., Ackerson, L.C., Klapstein, G.J. *et al.* (2003) Parkin-deficient mice exhibit nigrostriatal deficits but not loss of dopaminergic neurons. *J. Biol. Chem*, **278**, 43628–43635.
20. Selimi, F., Doughty, M., Delhaye-Bouchaud, N. and Mariani, J. (2000) Target-related and intrinsic neuronal death in lurcher mutant mice are both mediated by caspaea-3 actvation. *J. Neurosci.*, **20**, 992–1000.
21. Bando, Y., Tsukamoto, Y., Katayama, T., Ozawa, K., Kitao, Y., Hori, O., Stern, D.M., Yamauchi, A. and Ogawa, S. (2004) ORP150/HSP12A protects renal tubular epithelium from ischemia-induced cell death. *FASEB J.*, **18**, 1401–1403.
22. Lavoie, M.J., Ostaszewski, B.L., Weihofen, A., Schlossmacher, M.G. and Selkoe, D.J. (2005) Dopamine covalently modifies and functionally inactivates parkin. *Nat. Med.*, **11**, 1214–1221.
23. Cahill, A.L. and Ehret, C.F. (1982) Alpha-methyl-p-tyrosine shifts circadian temperature rhythms. *Am. J. Physiol.*, **243**, R218–R222.
24. Ko, H.S., vonCoelln, R., Sriram, S.R., Kim, S.W., Chung, K.K., Pletnikova, O., Troncoso, J., Johnson, B., Saffary, R., Goh, E.L. *et al.* (2005) Accumulation of the authentic parkin substrate aminoacyl-tRNA synthetase cofactor, p38/JTV-1, leads to catecholaminergic cell death. *J. Neurosci.*, **25**, 7968–7978.
25. Barkats, M., Bilang-Bleuel, A., Buc-Caron, M.H., Castel-Barthe, M.N., Corti, O., Finiels, F., Horellou, P., Revah, F., Sabate, O. and Mallet, J. (1998) Adenovirus in the brain: recent advances of gene therapy for neurodegenerative diseases. *Prog. Neurobiol.*, **55**, 333–341.
26. Gomi, H., Yokoyama, T., Fujimoto, K., Ikeda, T., Katoh, A., Itoh, T. and Itohara, S. (1995) Mice devoid of the glial fibrillary acidic protein develop normally and are susceptible to scrapie prions. *Neuron*, **14**, 29–41.
27. Yanagawa, Y., Kobayashi, T., Ohnishi, M., Kobayashi, T., Tamura, S., Tsuzuki, T., Sanbo, M., Yagi, T., Tashiro, F. and Miyazaki, J. (1999) Enrichment and efficient screening of ES cells containing a targeted mutation: the use of DT-A gene with the polyadenylation signal as a negative selection maker. *Transgenic Res.*, **8**, 215–221.
28. Namikawa, K., Murakami, K., Okamoto, T., Okado, H. and Kiyama, H. (2006) A newly modified SCG10 promoter and Cre/loxP-mediated gene amplification system achieve highly specific neuronal expression in animal brains. *Gene Ther.*, **13**, 1244–1250.
29. Satoh, T., Furuta, K., Tomokiyo, K., Nakatsuka, D., Tanikawa, M., Nakanishi, M., Miura, M., Tanaka, S., Koike, T., Hatanaka, H. *et al.* (2000) Facilitatory roles of novel compounds designed from cyclopentenone prostaglandins on neurite outgrowth-promoting activities of nerve growth factor. *J. Neurochem.*, **75**, 1092–1102.
30. Kuwabara, K., Matsumoto, M., Ikeda, J., Hori, O., Ogawa, S., Maeda, Y., Kitagawa, K., Imuta, N., Kinoshita, K., Stern, D. *et al.* (1996) Purufucation and characterization of a novel stress protein, the 150 kDa oxygen regulated protein (ORP150), from cultured rat astrocytes, and its expression in ischemic mouse brain. *J. Biol. Chem.*, **279**, 5025–5032.
31. Kuhn, K., Wellen, J., Link, N., Maskri, L., Lubbert, H. and Stichel, C.C. (2003) The mouse MPTP model: gene expression changes in dopaminergic neurons. *Eur. J. Neurosci.*, **17**, 1–12.
32. Itoh, S., Katsuura, G. and Takashima, A. (1988) Effect of vasoactive intestinal peptide on dopaminergic system in the rat brain. *Peptides*, **9**, 315–317.

BRAIN RESEARCH 1135 (2007) 195–200

available at www.sciencedirect.com

ScienceDirect

www.elsevier.com/locate/brainres

BRAIN RESEARCH

Research Report

Expression of S100 protein and protective effect of arundic acid on the rat brain in chronic cerebral hypoperfusion

Ryo Ohtani, Hidekazu Tomimoto , Hideaki Wakita, Hiroshi Kitaguchi, Kayoko Nakaji, Ryosuke Takahashi

Department of Neurology, Kyoto University Graduate School of Medicine, Shogoin, Sakyo-ku, Kyoto 606-8507, Japan

ARTICLE INFO

Article history:
Accepted 30 November 2006
Available online 8 January 2007

Keywords:
White matter
Chronic cerebral hypoperfusion
Apoptosis
Astroglia
S100 protein
Arundic acid

ABSTRACT

S100 protein is expressed primarily by astroglia in the brain, and accumulates in and around the ischemic lesions. Arundic acid, a novel astroglia-modulating agent, is neuroprotective in acute cerebral infarction, whereas the protective effects remain unknown during chronic cerebral hypoperfusion. Rats undergoing chronic cerebral hypoperfusion were subjected to a bilateral ligation of the common carotid arteries, and were allowed to survive for 3, 7 and 14 days. The animals received a daily intraperitoneal injection of 5.0, 10.0 or 20.0 mg/kg of arundic acid, or vehicle, for 14 days. Alternatively, other groups of rats received a delayed intraperitoneal injection of 20.0 mg/kg of arundic acid or vehicle, which started from 1, 3 or 7 days after ligation and continued to 14 days. The degree of white matter (WM) lesions and the numerical density of S100 protein-immunoreactive astroglia were estimated. In the WM of rats with vehicle injections, the number of S100 protein-immunoreactive astroglia increased significantly after chronic cerebral hypoperfusion as compared to the sham-operation. A dosage of 10.0 and 20.0 mg/kg of arundic acid suppressed the numerical increase in S100 protein-immunoreactive astroglia and the WM lesions. These pathological changes were suppressed with delayed treatment up to 7 days in terms of astroglial activation, and up to 3 days in terms of the WM lesions. The protective effects of arundic acid against WM lesions were demonstrated in a dose-dependent manner, and even after postischemic treatments. These results suggest the potential usefulness of arundic acid in the treatment of cerebrovascular WM lesions.

1. Introduction

Ischemic white matter (WM) lesions are frequently observed in human cerebrovascular diseases (CVD), and are believed to be responsible for cognitive impairments in the elderly. It is believed that the occlusion of the small vessels results in lacunar cerebral infarction, and non-occlusive arteriopathy causes chronic cerebral hypoperfusion and WM lesions (Pantoni and Garcia, 1997). Indeed, WM lesions can be induced by a ligation of the bilateral common carotid arteries (CCAs) in rats, which leads to a 50–70% decrease in normal cerebral blood flow (CBF) over an extended period of time (Tsuchiya

Corresponding author. Fax: +81 75 751 3766.
E-mail address: tomimoto@kuhp.kyoto-u.ac.jp (H. Tomimoto).

Abbreviations: WM, white matter; CVD, cerebrovascular disease; CCAs, common carotid arteries; CBF, cerebral blood flow; iNOS, inducible nitric oxide synthase; PBS, phosphate-buffered saline; KB, Klüver–Barrera; BBB, blood–brain barrier; TNF , tumor necrosis factor alpha; COX2, cyclooxygenase 2

0006-8993/$ – see front matter © 2006 Elsevier B.V. All rights reserved.
doi:10.1016/j.brainres.2006.11.084

et al., 1992; Wakita et al., 1994). The myelins become rarefied with a proliferation of the astroglia and an activation of microglia, plus oligodendroglial cell death with DNA fragmentation in the WM (Tomimoto et al., 2003).

S100 is a 20-kDa Ca-binding protein composed of and subunits, and is primarily expressed by astroglia in the brain. This protein may play a dual role in the regulation of cell function, being beneficial to cells at low doses but detrimental at high doses (Hu et al., 1996). In human CVD, a significant correlation has been reported between the plasma concentration of S100 protein and the volume of the cerebral infarct (Aurell et al., 1991). Although low concentrations of S100 protein protect cultured neurons from glutamate-induced excitotoxic damage, a high concentration of this protein upregulates the expression of inducible nitric oxide synthase (iNOS) in cultured astroglia with the subsequent production of NO and death of astroglia and neurons (Hu et al., 1996, 1997; Murphy, 2000).

Indeed, arundic acid, an agent that inhibits the astrocytic synthesis of S100 (Asano et al., 2005), has been shown to be neuroprotective in a rat model of acute cerebral infarction (Tateishi et al., 2002). Arundic acid may interfere with the intricate pathways of astrocytic activation upstream to the mRNA expression of various proteins, and is considered to be a modulator of the gene expression and functions of astroglia (Asano et al., 2005; Shinagawa et al., 1999).

In the present study, we examined the protective effects of arundic acid on WM lesions during chronic cerebral hypoperfusion, and also investigated its therapeutic window for delayed treatment. Our results support the potential use of arundic acid as a therapeutic intervention in human cerebrovascular WM lesions with cognitive impairment.

2. Results

2.1. *Mortality rates and laboratory data*

In the first series of experiments, 1 out of 7 arundic acid-treated rats died at a dosage of 5.0 mg/kg (14.3%), and none died at dosages of 10.0 and 20.0 mg/kg (0.0%). The laboratory data (erythrocyte count, leukocyte count, GOT, GPT, BUN and creatinine levels) and rectal temperature were not significantly different between the vehicle-treated and arundic acid-treated rats (Table 1).

2.2. *Dose-dependent effect of arundic acid on S100 protein expression*

In the WM of the sham-operated animals, only a few astroglia showed positive immunostaining for the S100 protein. From 3 to 14 days after the operation, the brains of the vehicle-treated animals showed a numerical increase in astroglia, which were immunoreactive for S100 protein in various WM regions such as the optic nerve, optic tract, corpus callosum, and internal capsule (Figs. 1A–D). These S100 protein-immunoreactive astroglia increased in number after BCAO as compared to the sham-operated control group in these WM regions (Fig. 1E, Table 2).

In the 10.0 and 20.0 mg/kg arundic acid-treated rats, S100 protein-immunoreactive astroglia appeared to be less numerous in the WM regions as compared to the vehicle-treated animals for 14 days. In the semi-quantitative analysis, the number of S100 protein-immunoreactive astroglia was reduced in both 10.0 and 20.0 mg/kg arundic acid-treated groups as compared to the vehicle-treated group ($p<0.001$; Figs. 2A–D). The number of astroglia decreased in the 5.0, 10.0 and 20.0 mg/kg arundic acid-treated groups compared to the vehicle-treated group. The number was also reduced in the 20.0 mg/kg arundic acid-treated animals as compared to the 10.0 mg/kg arundic acid-treated animals ($p<0.05$), indicating a dose-dependent effect for arundic acid (Fig. 2E, Table 2).

2.3. *Dose-dependent effect of arundic acid on WM lesions*

This dose-related protective effect was similarly observed with respect to the WM lesions. In the 10.0 and 20.0 mg/kg arundic acid-treated groups, the scores were lower as compared to the vehicle-treated group (two-factor factorial ANOVA; $p<0.001$). There were no significant differences in grading scores between the 5.0 mg/kg arundic acid-treated group and vehicle-treated group. However, the 20.0 mg/kg arundic acid-treated animals showed a significant reduction ($p<0.05$) as compared to the 10.0 mg/kg arundic acid-treated animals (Fig. 2F, Table 2).

2.4. *Effects of delayed treatment*

In the delayed-treatment group, which started from 1, 3, or 7 days after the operation, the number of S100 protein-immunoreactive astroglia showed a significant decrease in the WM regions as compared to the vehicle-treated animals

Table 1 – Summary of the laboratory data in rats receiving vehicle or arundic acid

	Erythrocyte ($\times 10^4$/mm^3) ($n=6$)	Leukocyte ($\times 10^2$/mm^3) ($n=6$)	Thrombocyte ($\times 10^3$/mm^3) ($n=6$)	GOT (IU/l) ($n=5$)	GPT (IU/l) ($n=6$)	BUN (mg/dl) ($n=5$)	Creatinine (mg/dl) ($n=6$)	Rectal temperature (°C) ($n=6$)
Vehicle	753.0±42.8	48.4±8.6	88.6±9.6	156.8±18.8	53.6±6.6	20.4±2.8	0.48±0.08	36.5±0.5
Arundic acid (5.0 mg/kg)	790.0±36.8	52.5±22.8	90.4±10.8	178.6±20.4	49.6±8.8	21.8±2.2	0.54±0.12	36.6±1.0
Arundic acid (10.0 mg/kg)	778.0±20.4	50.8±16.8	92.4±9.6	148.8±22.4	45.2±6.8	18.6±1.9	0.46±0.09	36.5±1.0
Arundic acid (20.0 mg/kg)	774.4±31.8	54.8±18.6	91.4±14.4	166.6±38.4	51.2±9.2	19.8±2.4	0.52±0.14	36.6±0.5

Values represent means±SD. n, number of animals. No significant differences were detected in the laboratory data between the arundic acid-treated group and the vehicle-treated group.

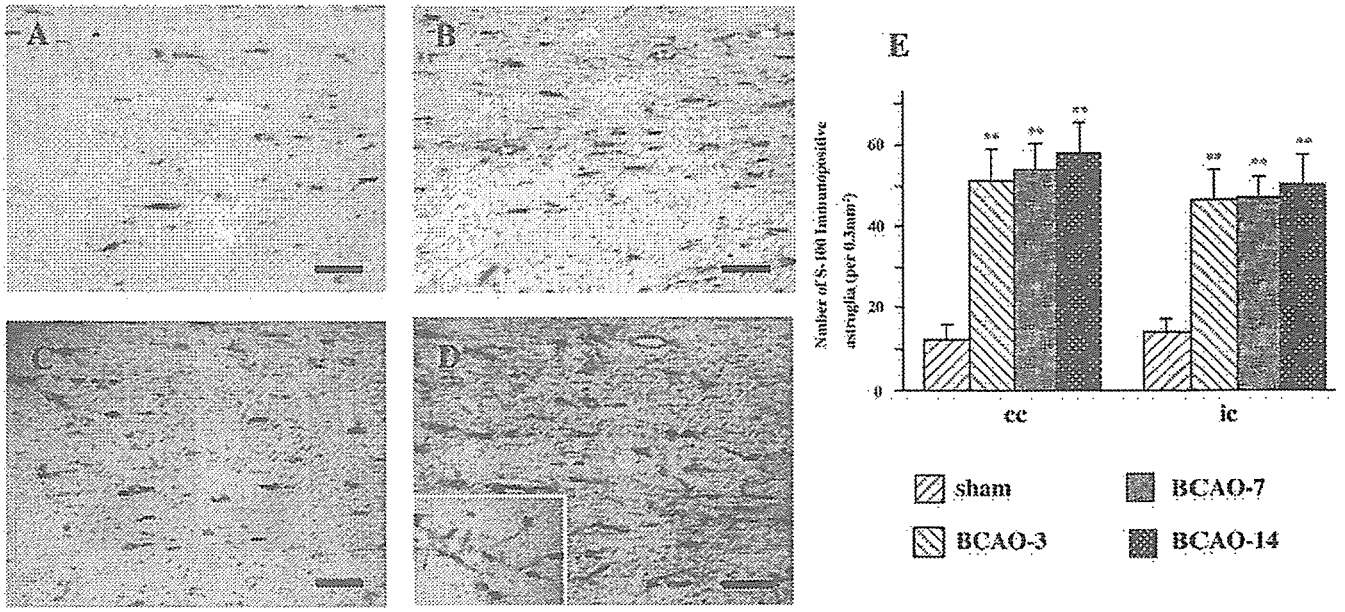

Fig. 1 – Photomicrographs of the immunohistochemical staining for S100 protein in the corpus callosum. The rats were subjected to a sham operation (A), or bilateral ligation of the carotid arteries for 3 days (B), 7 days (C) or 14 days (D). An inset in (D) indicates that S100 protein is intensely expressed in astroglial foot processes around the blood vessel. Bars indicate 100 m. E: Histograms of the numerical densities of S100 protein-immunoreactive astroglia in the WM of the rats after a bilateral common carotid artery occlusion. Six animals were used in each group. The asterisks indicate statistical significance at $p<0.01$ by Mann–Whitney *U* test when compared with the sham-operated controls. cc, corpus callosum; ic, internal capsule.

for 14 days (Figs. 3A–E, Table 2). The WM lesions were less severe (two-factor factorial ANOVA; $p<0.001$) as compared to the vehicle-treated group in the groups starting at 1 day and 3 days after the operation (Fig. 3F, Table 2), but there were no significant changes in the group starting at 7 days.

3. Discussion

In the present study, we demonstrated a protective effect for arundic acid against astroglial activation and WM lesions during chronic cerebral hypoperfusion. Arundic acid suppressed both the activation of the astroglia and the WM lesions in a dose-dependent manner. Both the astroglial activation and WM lesions were suppressed at dosages over 10 mg/kg, whereas the dosage of 5.0 mg/kg suppressed the astroglial activation exclusively. Therefore, it is unlikely that the activation of the astroglia was secondary to the WM damage, but rather seems to be related to the causative mechanism.

Microglia and astroglia are activated in the WM aberrantly after chronic cerebral hypoperfusion (Wakita et al., 1994). This activation occurs in a manner that predicts the extent and severity of the subsequent WM damage, suggesting an important role of glial activation in the pathogenesis of WM lesions. In the susceptible WM, apoptosis of the oligodendroglia is induced with an upregulation of inflammatory cytokines including tumor necrosis factor alpha (TNF), and free radicals released from activated microglia and astroglia (Tomimoto et al., 2003). In addition, the compromised BBB (Ueno et al., 2002) may allow the entry of macromolecules and other blood constituents such as proteases, immunoglobulins, complements, and cytokines into the perivascular WM tissues.

In studies using a neuronal and astroglia co-culture system, a high concentration of S100 protein upregulated NO release from the astroglia, which was shown to be neurotoxic

Table 2 – The number of S100 protein-immunoreactive astroglia in the white matter

	Corpus callosum				Internal capsule			
I. Temporal profile after BCAO	Sham	3 days	7 days	14 days	Sham	3 days	7 days	14 days
	12.3±3.5	51.3±7.8	53.8±6.9	58.1±7.3	14.0±3.6	46.5±7.7	47.0±5.2	50.5±7.1
II. Dose-dependent effect	Vehicle	5 mg/kg	10 mg/kg	20 mg/kg	Vehicle	5 mg/kg	10 mg/kg	20 mg/kg
	63.5±8.3	53.1±6.3	35.3±6.2	10.9±6.0	54.9±8.4	33.0±7.1	26.1±5	21.9±5.7
III. Effects of delayed treatment	Vehicle	Day 1	Day 3	Day 7	Vehicle	Day 1	Day 3	Day 7
	62.0±6.6	13.2±3.8	18.2±5.1	48.9±6.6	54.5±7.1	21.9±3.1	23.7±5.0	42.2±6.3

Values represent the number of S100 protein-immunoreactive astroglia in 0.3 mm^2 (means±SD).
$p<0.01$ compared to the sham-operated (I) and the vehicle-treated (II and III) animals.

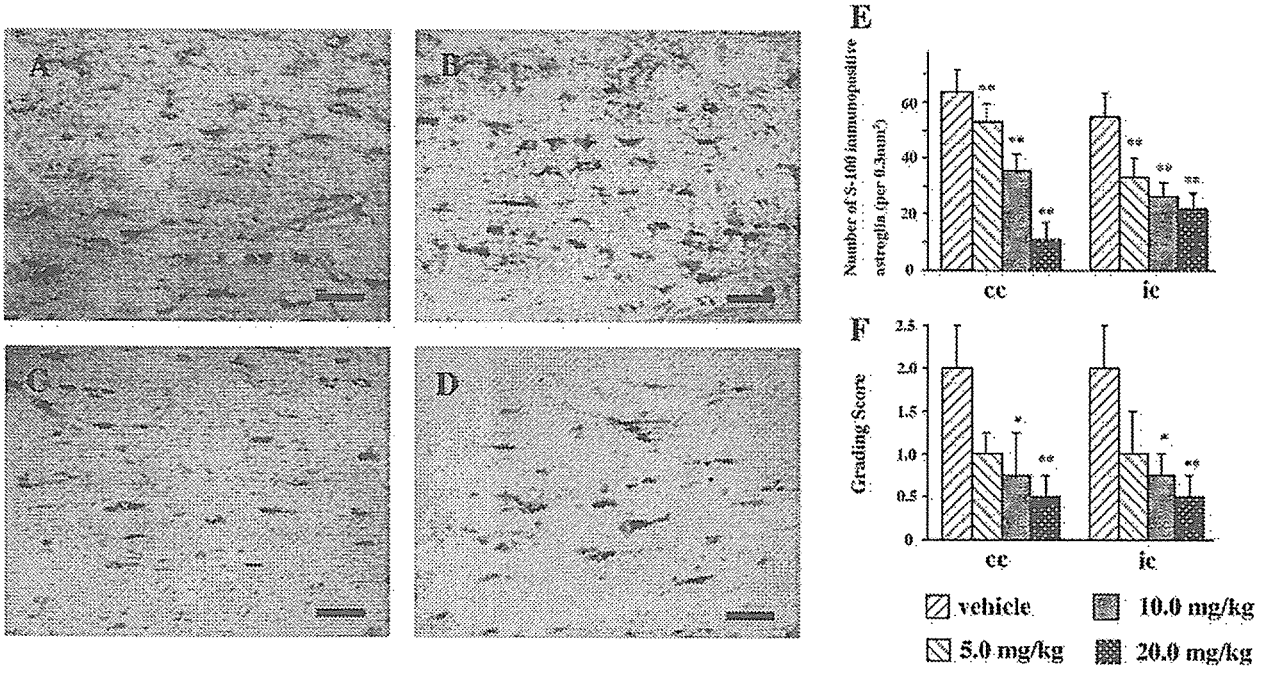

Fig. 2 – Photomicrographs of the immunohistochemical staining for S100 protein in the corpus callosum. The animals received an intraperitoneal injection of vehicle (A) or 5.0 mg/kg (B), 10.0 mg/kg (C) and 20.0 mg/kg (D) of arundic acid for 14 days. In the arundic acid-treated animals, astroglia immunoreactive for S100 protein were less numerous as compared with the vehicle-treated animals. Bars indicate 100 m. The histograms show the numerical densities of S100 protein-immunoreactive astroglia (E), and the grading scores for the WM lesions (F) in rats receiving either vehicle or arundic acid for 14 days. $^{*}p<0.05$; $^{**}p<0.01$ by Fisher's protected least significant difference procedure, as compared to the vehicle-treated animals.

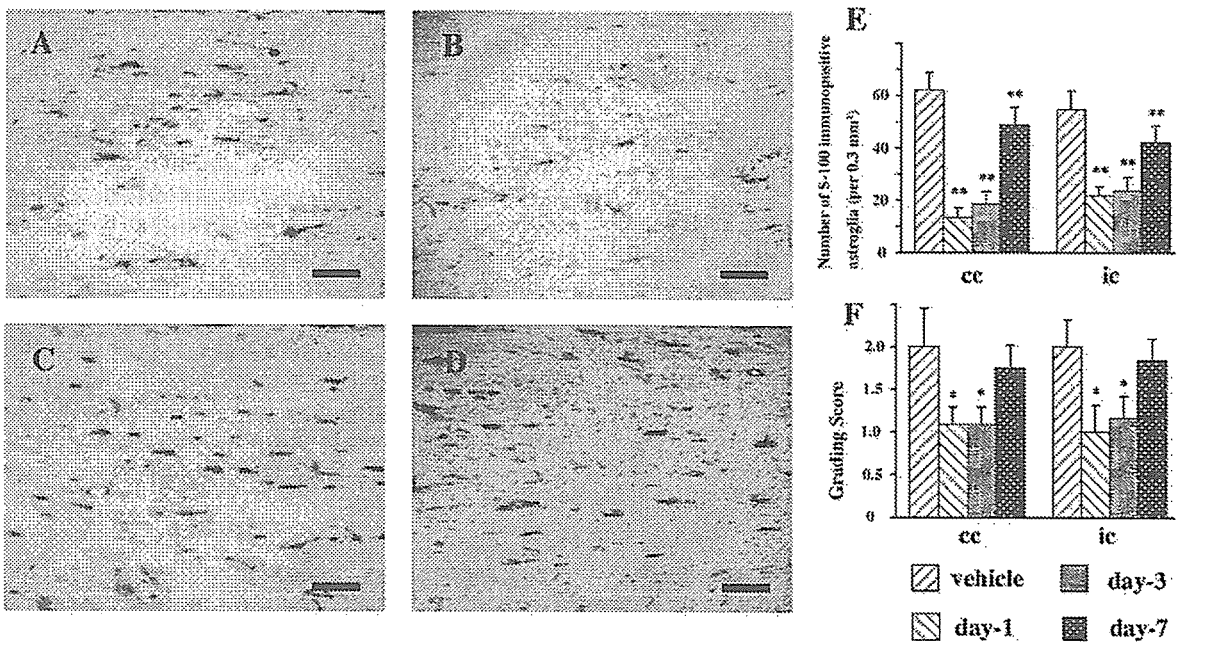

Fig. 3 – Photomicrographs of the immunohistochemical staining for S100 protein in the corpus callosum. The animals received an intraperitoneal injection of 20.0 mg/kg of arundic acid from 1 day (B), 3 days (C) or 7 days (D) after the operation, until 14 days. The control animals (A) received a daily injection of vehicle 1 day before the operation until 14 days. In the delayed treatment with arundic acid, the number of S100 protein-immunoreactive astroglia was significantly reduced as compared with the control animals. Bars indicate 100 m. The histograms show the numerical density of S100 protein-immunoreactive astroglia (E) and the grading scores for the WM lesions (F) in rats receiving either vehicle or arundic acid from 1 day, 3 days or 7 days after the operation until 14 days. $^{*}p<0.05$; $^{**}p<0.01$ by Fisher's protected least significant difference procedure, as compared to the vehicle-treated animals.

(Hu et al., 1997; Nawashiro et al., 2000). Although the mechanism of responsible for this astroglial activation by a low concentration of S100 protein remains unclear, this protein is believed to be further activated by a positive feedback loop (Guo et al., 2001; Murphy, 2000). It is postulated that these excessively activated astroglia may cause secondary tissue damage by the production of cytotoxic cytokines such as TNF , and cyclooxygenase 2 (COX2) and iNOS (Lam et al., 2001; Sharp et al., 2000). Indeed, the delayed expansion of the cerebral infarction was accompanied by astroglial activation as well as by an increased tissue level of S100 protein in the peri-infarct area. Thus, the astroglial overexpression of S100 protein is considered to play a pivotal role in infarct expansion by causing alterations in the activities of multiple intracellular signaling pathways and the expression of various downstream proteins (Asano et al., 2005; Matsui et al., 2002).

Several *in vitro* and *in vivo* studies have determined the pharmacological actions of arundic acid on astroglia. Arundic acid acts selectively on astroglia and modulates their activation, or prevents excessive activation that may be harmful to neighboring neurons. It does not act on neuronal cultures directly, but suppresses the changes induced in the co-cultured astroglia, such as an increase in S100 content, the secretion of nerve growth factor, a reduction in glutamate transporter (GLT-1 and GLAST) expression and the disappearance of GABAA receptors, in a dose-dependent manner, without affecting GFAP expression (Asano et al., 2005; Himeda et al., 2006; Katsumata et al., 1999; Matsui et al., 2002). In addition, arundic acid inhibits the expression of cyclooxygenase-2 or inducible nitric oxide synthase mRNA induced by lipopolysaccharide in cultured astroglia (Shimoda et al., 1998).

The dosage ranging from 5 to 20 mg/kg in the present study was comparable to that used in clinical application (8 mg/kg/h in acute stroke patients) (Pettigrew et al., in press). Furthermore, arundic acid was effective in delayed treatment starting from 7 days in terms of astroglial activation, and 3 days in terms of the WM lesions. This broad therapeutic time window is of clinical relevance, because the patients with subcortical vascular dementia, a form of vascular dementia characterized by diffuse WM lesions, frequently undergo a latent deterioration and hospitalization delay (Roman, 2005).

4. Experimental procedures

4.1. *Animals*

Chronic cerebral hypoperfusion was induced in male Wistar rats (150 to 200 g; Shimizu Laboratory Supplies Co. Ltd., Kyoto, Japan) as previously described (Wakita et al., 1994). The animals were anesthetized with sodium pentobarbital (25 mg/kg, i. p.) and were allowed spontaneous respiration throughout the surgical procedure. Through a midline cervical incision, both CCAs were exposed and double-ligated with silk sutures. Their rectal temperature was monitored and maintained between 36.0 and 37.0 °C during the surgical procedure, and the rats were kept in animal quarters with standard rodent chow and tap water *ad libitum* after the operation.

4.2. *Treatment with arundic acid*

The rats with vehicle (saline) treatment were sacrificed at 3, 7 and 14 days (body weight, 300 g; $n=6$, for each group) to study the temporal profile of the S100 protein-immunoractive astroglia and the WM lesions. In the first series of experiments with arundic acid, the animals received a daily intraperitoneal injection of 5.0, 10.0 or 20.0 mg/kg of arundic acid, or vehicle, from 1 day before the operation to 14 days afterwards ($n=6$ for each group). At 14 days after ligation, the animals were sacrificed and subjected to the experiments detailed below. The sham-operated animals were treated similarly to the operated ones, except the CCAs were not occluded. In the second series with a delayed-treatment, the animals received a daily intraperitoneal injection of 20.0 mg/kg of arundic acid or vehicle from 1 day, 3 days or 7 days after the operation until 14 days ($n=6$ for each group). At 14 days after ligation, the animals were sacrificed and subjected to the experiments detailed below. The control animals received a daily injection of vehicle 1 day after the operation until 14 days.

4.3. *Standard histological and immunohistochemical study*

After the operation, the animals were deeply anesthetized with sodium pentobarbital and were perfused transcardially with 0.01 mol/L phosphate-buffered saline (PBS), and then with a fixative containing 4% paraformaldehyde and 0.2% picric acid in 0.1 mol/L PB (pH 7.4). The brains were then stored in 20% sucrose in 0.1 mol/L PBS (pH 7.4). These specimens were embedded in paraffin and sliced into 2 m-thick coronal sections. Klüver–Barrera (KB) staining was used to observe any histological changes. The severity of the WM lesions was graded as normal (grade 0), disarrangement of the nerve fibers (grade 1), formation of vacuoles (grade 2) and loss of myelinated fibers (grade 3) by two independent investigators blinded to the type of treatment, as described elsewhere (Wakita et al., 1994). For the immunohistochemistry, polyclonal antibodies directed against the S100 protein (diluted 1:1000; Dakopatts, 4.5 mg/L) were used in the present study. After incubation with the primary antibodies, the sections were treated with a biotinylated anti-rabbit antibody (IgG) (diluted 1:200; Vector Laboratories), and an avidin biotin complex (diluted 1:200; Vector Laboratories) in 20 mmol/L PBS containing 0.3% Triton-X. The sections were finally incubated in 0.01% diaminobenzidine tetrahydrochloride and 0.005% H_2O_2 in 50 mmol/L Tris HCl (pH 7.6). To test the specificity of the immunohistochemical reaction, coronal sections were treated with normal mouse IgG instead of the primary antibodies. The number of nuclei with S100 protein-immunoreactive cytoplasm was counted against a square test grid in 20 representative fields (per 0.3 mm^2) of the corpus callosum and internal capsule ($n=6$) by two independent investigators blinded to the type of treatments as described previously (Tomimoto et al., 1996).

4.4. *Statistical analysis*

The data were expressed as means ± SD. Differences in rectal temperature between the groups were determined by a

repeated-measure ANOVA. Differences in terms of laboratory blood data were determined by a one-factor ANOVA between each group. Differences in the grading scores were determined by a two-factor factorial ANOVA followed by Fischer's protected least significant difference procedure between each group. The Kruskal–Wallis test followed by post-hoc test was used to compare the ischemic group with the sham-operated control group in the semiquantification for S100 protein-immunoreactive astroglia. A p value of <0.05 was considered to be statistically significant.

Acknowledgments

We appreciatively acknowledge Ono Pharmaceutical Co. Ltd., Osaka, Japan, for providing arundic acid (ONO-2506), and for helpful advice. This study was supported by a grant-in-aid for scientific research (C) (18590936) from the Japanese Ministry of Education, Culture, Sports, Science and Technology to H. T. and Dr. H. Saiki (Kitano Hospital, Osaka, Japan).

REFERENCES

Asano, T., Mori, T., Shimoda, T., Shinagawa, R., Satoh, S., Yada, N., Katsumata, S., Matsuda, S., Kagamiishi, Y., Tateishi, N., 2005. Arundic acid (ONO-2506) ameliorates delayed ischemic brain damage by preventing astrocytic overproduction of S100B. Curr. Drug Targets, CNS Neurol. Disord. 4, 127–142.

Aurell, A., Rosengren, E.L., Larlsson, B., Olsson, E.J., Zbornikova, V., Haglid, G.K., 1991. Determination of S-100 and glial fibrillary acidic protein concentrations in cerebrospinal fluid after brain infarction. Stroke 22, 1254–1258.

Guo, L., Sawkar, A., Zasadzki, M., Watterson, M.D., 2001. Similar activation of glial cultures from different rat brain regions by neuroinflammatory stimuli and downregulation of the activation by a new class of small molecule ligands. Neurobiol. Aging 22, 975–981.

Himeda, T., Kadoguchi, N., Kamiyama, Y., Kato, H., Maegawa, H., Araki, T., 2006. Neuroprotective effect of arundic acid, an astrocyte-modulating agent, in mouse brain against MPTP (1-methyl-4-phenyl-1,2,3,6-tetrahydropyridine) neurotoxicity. Neuropharmacology 50, 329–344.

Hu, J., Castets, F., Guevana, L.J., 1996. S100 stimulates inducible nitric oxide synthase activity and mRNA levels in rat cortical astrocytes. J. Biol. Chem. 271, 2543–2547.

Hu, J., Ferreia, A., 1997. S100 induces neuronal cell death through nitric oxide release from astrocytes. J. Neurochem. 69, 2294–2301.

Katsumata, S., Tateishi, N., Kagamiishi, Y., Shintaku, K., Hayakawa, T., Shimoda, T., Shinagawa, R., Akiyama, T., Katsube, N., 1999. Inhibitory effect of ONO-2506 on GABAA receptor disappearance in cultures astrocytes and ischemic brain. Abstr.-Soc. Neurosci. 25, 2108.

Lam, G.A., Koppal, T., Akama, T.K., Guo, L., Craft, M.J., Samy, B., Schavocky, P.J., Watterson, M.D., 2001. Mechanism of glial activation by S100B: involvement of the transcription factor NF B. Neurobiol. Aging 22, 765–772.

Matsui, T., Mori, T., Tateishi, N., Kagamiishi, Y., Satoh, S., Katsube, N., Morizawa, E., Morimoto, T., Ikuda, F., Asano, T., 2002. Astrocytic activation and delayed infarct expansion after permanent focal ischemia in rats. Part 1: enhanced astrocytic synthesis of S100 in the periinfarct area precedes delayed infarct expansion. J. Cereb. Blood Flow Metab. 22, 711–722.

Murphy, S., 2000. Production of nitric oxide by glial cells: regulation and potential roles in the CNS. Glia 29, 1–13.

Nawashiro, H., Brenner, M., Fukui, S., Shima, K., Hallenbeck, M.J., 2000. High susceptibility to cerebral ischemia in GFAP-null mice. J. Cereb. Blood Flow Metab. 20, 1040–1044.

Pantoni, H.J., Garcia, H.J., 1997. Pathogenesis of leukoaraiosis: a review. Stroke 28, 652–659.

Pettigrew, C.L., Kasner, E.S., Albers, W.G., Gorman, M., Grotta, C.J., Sherman, G.D., Funakoshi, Y., Ishibashi, H., for the arundic acid (ONO-2506) stroke study group, 2006. Safety and tolerability of arundic acid in acute ischemic stroke. J. Neurol. Sci. 251, 50–56.

Roman, C.G., 2005. Vascular dementia prevention: a risk factor analysis. Cerebrovasc. Dis. 20, 91–100.

Sharp, R.F., Lu, A., Tang, Y., Millhorn, E.D., 2000. Multiple molecular penumbras after focal cerebral ischemia. J. Cereb. Blood Flow Metab. 20, 1011–1032.

Shimoda, T., Tateishi, K., Shintaku, K., Yada, N., Katagi, J., Akiyama, T., Maekawa, H., Shinagawa, R., Kondo, K., 1998. ONO-2506, a novel astrocyte modulating agent, suppresses of COX-2 and iNOS mRNA expression in cultured astrocytes and ischemic brain. Abstr.-Soc. Neurosci. 24, 384.

Shinagawa, R., Tateishi, N., Shimoda, T., Maekawa, H., Yada, N., Akiyama, T., Matsuda, S., Katsube, N., 1999. Modulating effects of ONO-2506 on astrocytic activation in cultured astrocytes from rat cerebrum. Abstr.-Soc. Neurosci. 25, 843.

Tateishi, N., Mori, T., Kagamiishi, Y., Satoh, S., Katsube, N., Morizawa, E., Morimoto, T., Matsui, T., Asano, T., 2002. Astrocytic activation and delayed infarct expansion after permanent focal ischemia in rats. part 2: suppression of astrocytic activation by a novel agent (R)-(–)-2-propyloctanoic acid (ONO-2506) leads to mitigation of delayed infarct expansion and early improvement of neurologic deficits. J. Cereb. Blood Flow Metab. 22, 723–734.

Tomimoto, H., Akiguchi, I., Suenaga, T., Nishimura, M., Wakita, H., Nakamura, S., Kimura, J., 1996. Alterations of the blood–brain barrier and glial cells in white matter lesions in cerebrovascular and Alzheimer's disease patients. Stroke 27, 2069–2074.

Tomimoto, H., Ihara, M., Wakita, H., Ohtani, R., Lin, X.J., Akiguchi, I., Kinoshita, M., Shibasaki, H., 2003. Chronic cerebral hypoperfusion induces white matter lesions and loss of oligodendroglia with DNA fragmentation in the rat. Acta Neuropathol. (Berl.) 106, 527–534.

Tsuchiya, M., Sako, K., Yura, S., Yonemasu, Y., 1992. Cerebral blood flow and histopathological changes following permanent bilateral carotid artery ligation in Wistar rats. Exp. Brain Res. 89, 87–92.

Ueno, M., Tomimoto, H., Akiguchi, I., Wakita, H., Sakamoto, H., 2002. Blood–brain barrier is disrupted in the white matter lesions in a rat model of chronic cerebral hypoperfusion. J. Cereb. Blood Flow Metab. 22, 97–104.

Wakita, H., Tomimoto, H., Akiguchi, I., Kimura, J., 1994. Glial activation and white matter changes in the rat brain induced by chronic cerebral hypoperfusion: an immunohistochemical study. Acta Neuropathol. (Berl.) 87, 484–492.

BRAIN RESEARCH 1136 (2007) 219–227

available at www.sciencedirect.com

ScienceDirect

www.elsevier.com/locate/brainres

BRAIN RESEARCH

Research Report

Accumulation of Hsc70 and Hsp70 in glial cytoplasmic inclusions in patients with multiple system atrophy

Yasuhiro Kawamoto[a,*], *Ichiro Akiguchi*[a], *Yoshitomo Shirakashi*[a], *Yasuyuki Honjo*[a], *Hidekazu Tomimoto*[a], *Ryosuke Takahashi*[a], *Herbert Budka*[b]

[a]*Department of Neurology, Faculty of Medicine, Kyoto University, 54 Shogoin-Kawaharacho, Sakyoku, Kyoto 606-8507, Japan*
[b]*Institute of Neurology, Medical University Vienna, Vienna, Austria*

ARTICLE INFO

Article history:
Accepted 9 December 2006
Available online 22 December 2006

Keywords:
-Synuclein
Glial cytoplasmic inclusion
Hsc70
Hsp70
Multiple system atrophy

ABSTRACT

Heat shock proteins (HSPs) are molecular chaperones which can be induced by several kinds of stresses, and Hsc70 and Hsp70 are two major members of the family of 70 kDa HSPs. A major component of Lewy bodies (LBs) is -synuclein, and Hsp70 has been observed in the LBs of brains with Parkinson's disease. Hsp70 has also been demonstrated to have the ability to suppress -synuclein toxicity *in vitro* and *in vivo*. To investigate the precise role of Hsc70 and Hsp70 in patients with multiple system atrophy (MSA), which is another -synuclein-related disease, we performed immunohistochemical studies on Hsc70 and Hsp70 using autopsied brains from 7 normal subjects and 15 patients with MSA. In the normal human brains, both neurons and glial cells, including oligodendrocytes, showed only weak Hsc70 and Hsp70 immunoreactivities. In contrast, in the brains with MSA, numerous glial cytoplasmic inclusions (GCIs) were intensely immunostained with Hsc70, and strong Hsc70 immunoreactivity was also found in glial intranuclear inclusions (GNIs), neuronal cytoplasmic inclusions (NCIs) and neuronal intranuclear inclusions (NNIs) as well as dystrophic neurites. The immunolabeling pattern for Hsp70 in the MSA brains was slightly different from that of Hsc70, and Hsp70 immunoreactivity was observed in many reactive astrocytes as well as some glial and neuronal inclusions. Our results suggest that the widespread accumulation of Hsc70 and Hsp70 may occur in brains with MSA, and that Hsc70 and Hsp70 may be associated with the pathogenesis of MSA.

1. Introduction

Multiple system atrophy (MSA) is a single nosological entity which encompasses olivopontocerebellar atrophy (OPCA), striatonigral degeneration (SND) and Shy–Drager syndrome (SDS) (Graham and Oppenheimer, 1969). MSA is characterized clinically by varying degrees of autonomic failure, cerebellar ataxia, parkinsonism and pyramidal tract signs (Wenning et al., 1994). Recently, MSA has been divided into two groups: one group contains those patients with predominant cerebellar features

Corresponding author. Fax: +81 75 751 3265.
E-mail address: kawamoto@kuhp.kyoto-u.ac.jp (Y. Kawamoto).

Abbreviations: BCIP/NBT, 5-bromo-4-chloro-3-indolyl-phosphate/nitroblue tetrazolium; GCIs, glial cytoplasmic inclusions; GNIs, glial intranuclear inclusions; HSPs, heat shock proteins; LBs, Lewy bodies; MSA, multiple system atrophy; MSA-C, MSA of the cerebellar type; MSA-P, MSA of the parkinsonian type; NCIs, neuronal cytoplasmic inclusions; NNIs, neuronal intranuclear inclusions; OPCA, olivopontocerebellar atrophy; PD, Parkinson's disease; PVDF, polyvinylidene difluoride; SDS, Shy–Drager syndrome; SND, striatonigral degeneration

0006-8993/$ – see front matter © 2006 Elsevier B.V. All rights reserved.
doi:10.1016/j.brainres.2006.12.049

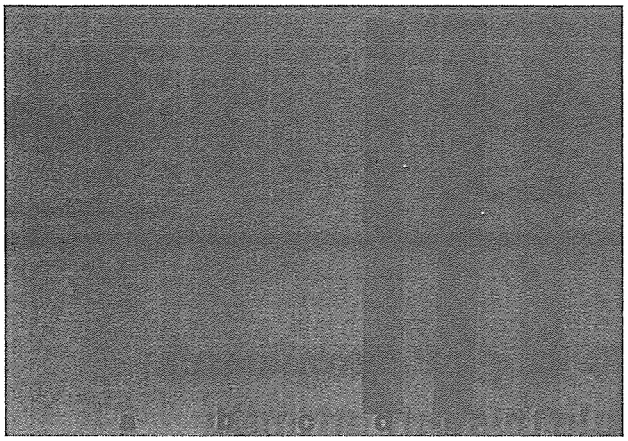

Fig. 1 – Western blot analysis of normal human brain homogenates (a, d), recombinant Hsp70 protein (b, e) and recombinant Hsc70 protein (c, f). Lanes a, b and c were incubated with the anti-Hsc70 antibody, and lanes d, e and f were incubated with the anti-Hsp70 antibody.

(MSA-C), and the other represents patients with predominant parkinsonian features (MSA-P) (Gilman et al., 1999). Specific oligodendroglial cytoplasmic inclusions, which are also referred to as glial cytoplasmic inclusions (GCIs), are the pathological hallmark of MSA (Nakazato et al., 1990; Papp et al., 1989), and the presence of GCIs strongly supports the concept of MSA as a single entity (Papp et al., 1989). GCIs are argyrophilic inclusions that can be detected at high sensitivity by the Gallyas silver staining technique (Papp et al., 1989), and are ultrastructurally composed of loosely packed filaments coated by granular materials (Nakazato et al., 1990; Papp et al., 1989).

Human -synuclein is a presynaptic protein of 140 amino acid residues (Jakes et al., 1994), and missense mutations in the -synuclein gene have been linked to some cases of autosomal dominant familial Parkinson's disease (PD) (Krüger et al., 1998; Polymeropoulos et al., 1997). Lewy bodies (LBs) are neuronal inclusions characteristic for PD (Pollanen et al., 1993), and -synuclein is a major component of both LBs (Spillantini et al., 1997; Wakabayashi et al., 1997, 1998b) and GCIs (Gai et al., 1998; Wakabayashi et al., 1998a,b); therefore, -synuclein-related disorders, including PD and MSA, are now collectively referred to as " -synucleinopathy". In addition to GCIs, -synuclein-immunopositive inclusions are also observed in the neuronal cytoplasm and nuclei of neurons and oligodendrocytes, and they are termed neuronal cytoplasmic inclusions (NCIs), neuronal intranuclear inclusions (NNIs) and glial intranuclear inclusions (GNIs), respectively (Lin et al., 2004; Wakabayashi et al., 1998a,b). Furthermore, a reduction in the solubility of -synuclein has been shown to occur in brains affected by MSA (Dickson et al., 1999; Tu et al., 1998). These data suggest that the neuronal and oligodendroglial accumulation of insoluble -synuclein may be closely related to the pathogenesis of MSA.

Heat shock proteins (HSPs) are molecular chaperones which are induced in response to heat shock, ischemia and other stresses (Ohtsuka and Suzuki, 2000; Sharp et al., 1999). The family of 70 kDa HSPs has two major members: Hsp70, an inducible form, and Hsc70, a constitutively expressed form (Ohtsuka and Suzuki, 2000; Sharp et al., 1999). The localization of Hsp70 in LBs from brains with PD has been previously reported (Auluck et al., 2002; Shin et al., 2005), and Hsp70 has been demonstrated to have the ability to suppress -synuclein toxicity *in vitro* (Dedmon et al., 2005; Klucken et al., 2004) and *in vivo* (Auluck et al., 2002; Klucken et al., 2004). However, the data regarding Hsc70 and Hsp70 in patients with MSA are very limited (Uryu et al., 2006), and therefore, we performed immunohistochemical studies on Hsc70 and Hsp70 using autopsied brains from patients with MSA. We observed the enhanced immunoexpression of both chaperones in those brains affected by MSA.

2. Results

2.1. *Western blot analysis*

A single band at a molecular weight of approximately 70 kDa was immunostained by the anti-Hsc70 antibody in the normal human cerebellar homogenate (Fig. 1a), and the anti-Hsc70 antibody also recognized the recombinant Hsc70 protein (Fig. 1c), but not the recombinant Hsp70 protein (Fig. 1b). On the other hand, a single band of about 70 kDa was immunolabeled with the anti-Hsp70 antibody in the normal human cerebellar homogenate (Fig. 1d), and the anti-Hsp70 antibody reacted with the recombinant Hsp70 antibody (Fig. 1e), but not the recombinant Hsc70 protein (Fig. 1f). Furthermore, both the antibodies detected only a single band of the same molecular weight in the cerebellar homogenate from the patient with MSA (Figs. 2a, b). These results indicate that the anti-Hsc70 and anti-Hsp70 antibodies were specific for human Hsc70 and Hsp70, respectively.

2.2. *Hsc70 and Hsp70 immunoreactivities in normal brains*

In the normal human brains, the neurons generally showed weak Hsc70 immunoreactivity (Fig. 3A), and faint Hsc70

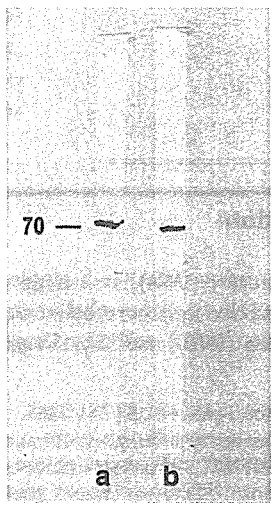

Fig. 2 – Western blot analysis of brain homogenates from the patient with multiple system atrophy. Lanes a and b were incubated with the anti-Hsc70 and anti-Hsp70 antibodies, respectively.

immunoreactivity was observed in a few glial cells, including oligodendrocytes (Fig. 3B).

The immunolabeling pattern of Hsp70 in the normal human brains was similar to that of Hsc70, and both neurons and glial cells were mildly immunoreactive for Hsp70 (Figs. 3C, D).

2.3. *Hsc70 immunoreactivity in brains with MSA*

In contrast to the weak Hsc70 immunoreactivity observed in the oligodendrocytes from the normal brains, numerous GCIs were intensely immunostained with Hsc70 in various lesions of the MSA brains, including the pontine nucleus (Fig. 4A), middle cerebellar peduncle (Fig. 4B) and cerebellar white matter (Fig. 4C). In addition, Hsc70-immunopositive GNIs, which consisted of a few filamentous structures, were found in some oligodendrocytes (Fig. 4D).

Similar to the normal controls, the remaining neurons were generally immunostained weakly in the brains with MSA, but strong Hsc70 immunoreactivity was localized throughout the cell bodies and proximal processes of some neurons (Fig. 4E). In the pontine and inferior olivary nuclei from the MSA cases, NCIs and NNIs in some surviving neurons were intensely immunolabeled (Figs. 4F, G). The NCIs were round or oval in shape (Fig. 4F), and the NNIs were wisps containing several filamentous structures (Fig. 4G). Furthermore, some dystrophic neurites were also densely immunoreactive for Hsc70 (Fig. 4H).

No significant difference was detected in the immunolabeling patterns of the neuronal and oligodendroglial inclusions between the MSA-C and MSA-P cases.

2.4. *Hsp70 immunoreactivity in brains with MSA*

Similar to Hsc70, the GCIs were intensely immunostained with Hsp70 (Figs. 5A, B), but serial sections immunostained alternately with the antibodies against Hsc70 and Hsp70 showed that the proportion of Hsp70-immunopositive GCIs was less than that of Hsc70-positive GCIs. The remaining neurons generally showed weak Hsp70 immunoreactivity (Fig. 5C), and some surviving neurons contained Hsp70-immunopositive NCIs (Fig. 5D). In comparison to Hsc70, the Hsp70-immunolabeled GNIs, NNIs and dystrophic neurites were very few. In addition to the oligodendrocytes, many reactive astrocytes were also strongly immunoreactive for Hsp70 (Fig. 5E), and immunopositive reactive astrocytes were distributed abundantly in the severely affected lesions, where the neuronal loss and astrogliosis were conspicuous (Fig. 5F). Hsp70-immunopositive reactive astrocytes were also observed in the areas where no -synuclein-positive inclusions were found. No significant difference was detected in the immunostaining patterns of the -synuclein-containing inclusions and reactive astrocytes between the MSA-C and MSA-P cases.

2.5. *Double-labeling immunohistochemistry for -synuclein and HSPs*

The double-immunofluorescence staining sections showed that -synuclein and Hsc70 were co-localized in most GCIs (Figs. 6A–C), and the co-localization of -synuclein and Hsp70 was also observed in some GCIs (Figs. 6D–F). No significant differences were detected in the co-localization of -synuclein and Hsc70 or Hsp70 in the GCIs among the cerebellat white matter, pontine base and putamen. The semiquantitative analyses demonstrated that the average percentage of Hsc70- or Hsp70-immunopositive GCIs in the -synuclein-immunolabeled GCIs was approximately 82.1% and 59.8%, respectively.

2.6. *Double-labeling immunohistochemistry for Hsc70 and glial markers*

The double-immunofluorescence staining sections revealed that Hsc70-immunopositive glial cells were mainly transferrin-

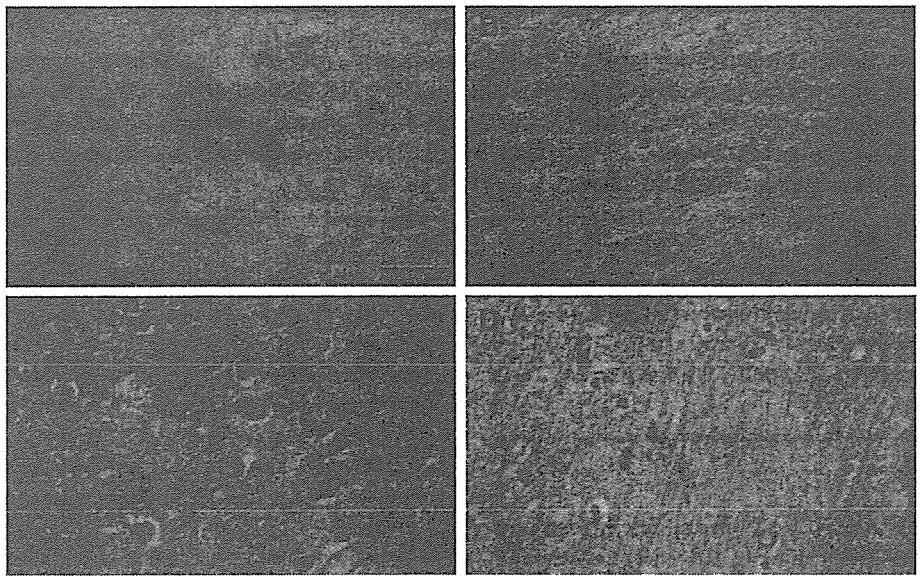

Fig. 3 – Immunohistochemical staining with Hsc70 (A: Control 3; B: Control 5) and with Hsp70 (C: Control 3; D: Control 5) in the normal pontine nucleus (A, C) and cerebellar white matter (B, D). Scale bars=50 m.

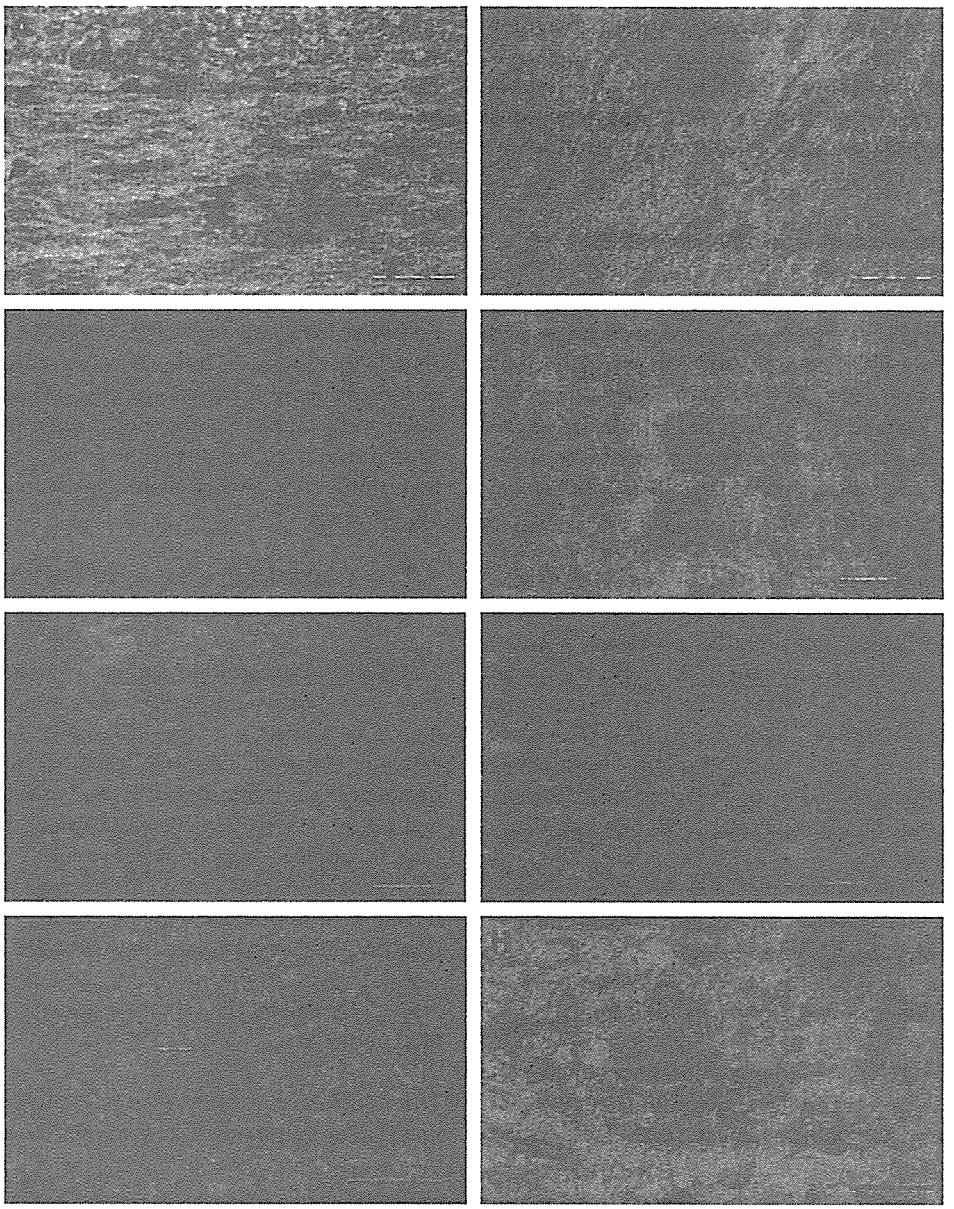

Fig. 4 – Immunohistochemical staining with Hsc70 in the pontine nucleus (A, D-H), middle cerebellar peduncle (B) and cerebellar white matter (C) from the patients with multiple system atrophy (A, C, H: MSA 2; B: MSA 3; D, F, G: MSA 11; E: MSA 14). Note that strong Hsc70 immunoreactivity was observed in the glial cytoplasmic inclusions (GCIs; A–C), glial intranuclear inclusions (GNIs; D, arrow), neuronal cytoplasmic inclusions (NCIs; F), neuronal intranuclear inclusions (NNIs; G, arrow) and dystrophic neurites (H). Scale bars = A–C, E 50 m; D 15 m; F–H 25 m.

positive oligodendrocytes (Figs. 7A–C). In contrast, very few Hsc70-immunopositive structures were located to glial fibrillary acidic protein (GFAP)-positive astrocytes (Figs. 7D–F) and leukocyte common antigen (LCA)-positive microglia (Figs. 7G–I).

3. Discussion

The widespread distribution of GCIs in the central nervous system is the main pathological feature of patients with MSA (Papp and Lantos, 1994). In the present study, we performed immunohistochemical studies on Hsc70 and Hsp70 using autopsied brains from 7 normal subjects and 15 patients with MSA, and then compared the immunostaining patterns between the two groups. We found that a few glial cells, including oligodendrocytes, showed weak Hsc70 and Hsp70 immunoreactivities in the normal brains, but the GCIs were strongly immunoreactive for Hsc70 and Hsp70 in the brains with MSA. Our observations suggest that Hsc70 and Hsp70 may be expressed aberrantly in oligodendrocytes, and may be associated with the formation of GCIs in those brains affected by MSA.

Recently, Uryu et al. (2006) demonstrated that among the various types of HSPs, Hsp90 was most prominently and consistently co-localized with -synuclein in LBs and GCIs, and in contrast to Hsp90, very few GCIs were immunopositive

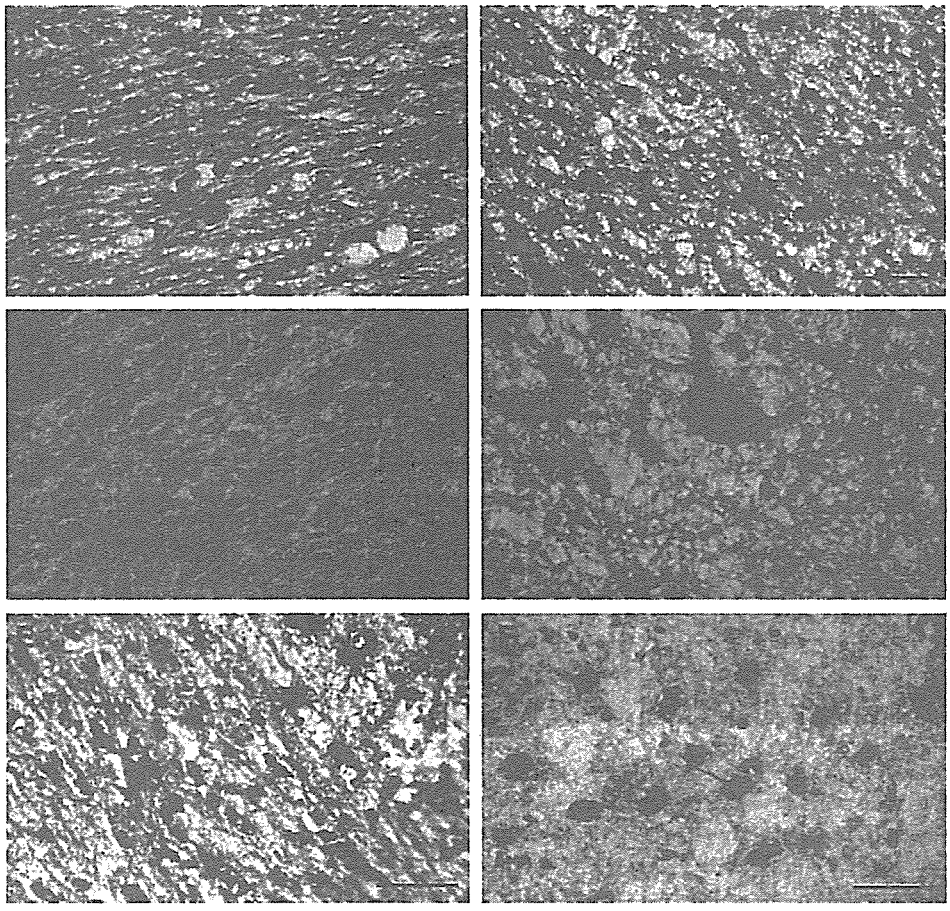

Fig. 5 – Immunohistochemical staining with Hsp70 in the pontine nucleus (A, C, D), cerebellar white matter (B) and putamen (E, F) from the patients with multiple system atrophy (A: MSA 2; B: MSA 3; C, E: MSA 11; D, F: MSA1). Some glial cytoplasmic inclusions (GCIs; A, B) and neuronal cytoplasmic inclusions (NCIs; D) were intensely immunostained. In contrast to the strongly immunopositive GCIs (C, arrows), the remaining neurons showed weak Hsp70 immunoreactivity (C). Reactive astrocytes as well as GCIs were immunoreactive for Hsp70 (E), and immunopositive reactive astrocytes were abundant in the severely affected areas (F). Scale bars = A–C, E, F 50 m; D 25 m.

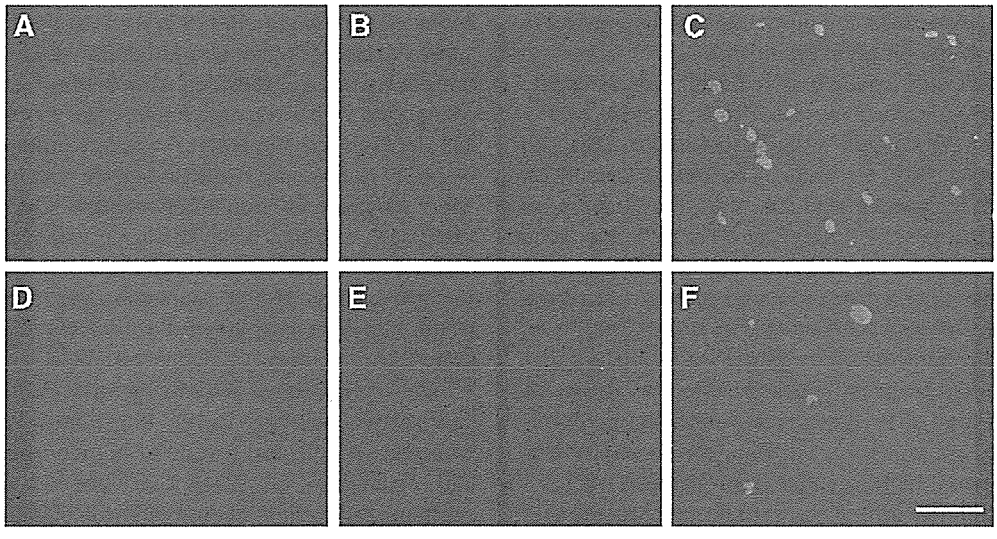

Fig. 6 – Double-immunofluorescence staining for -synuclein (A, D; red) and Hsc70 (B; green) or Hsp70 (E; green) in the cerebellar white matter from the patient with multiple system atrophy (MSA 3). The merged images showed that -synuclein and Hsc70 were co-localized in most glial cytoplasmic inclusions (GCIs; C), and -synuclein and Hsp70 were co-localized in some GCIs (F). Scale bar = F (also for A–E) 20 m.

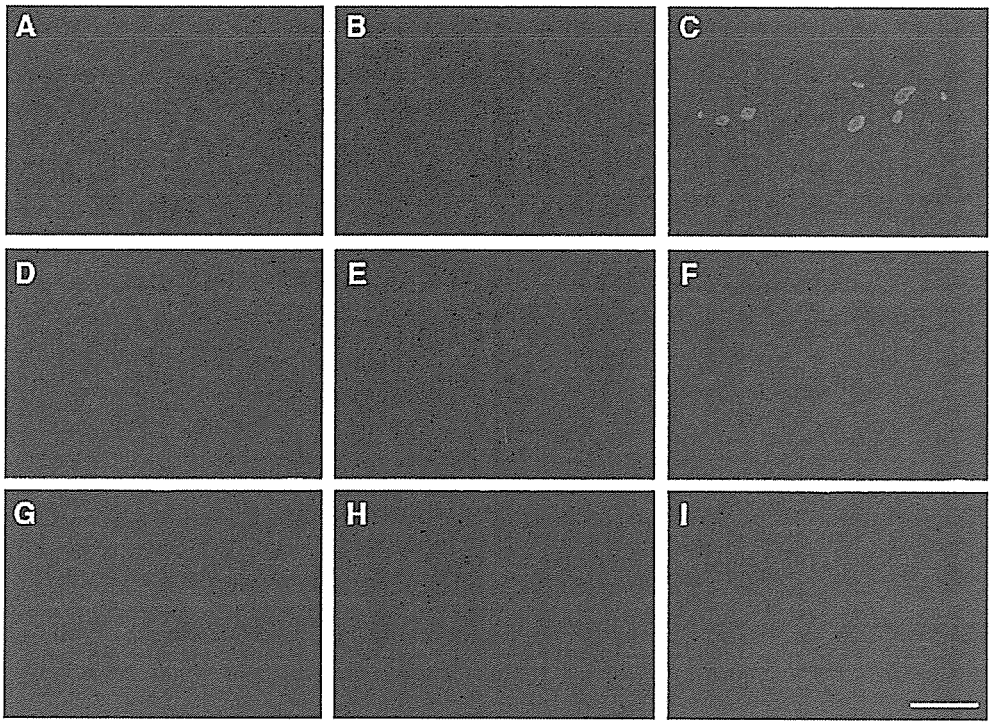

Fig. 7 – Double-immunofluorescence staining for Hsc70 (A, D, G; green) and transferrin (B; red), GFAP (E; red) or LCA (H; red) in the pontine base from the patient with multiple system atrophy (MSA 5). The merged images showed that Hsc70-immunopositive glial cells were mainly oligodendrocytes (C), and very few Hsc70-immunopositive structures were localized to astrocytes (F) and microglia (I). Scale bar=I (also for A–H) 20 m.

for Hsc70 and Hsp70. Conversely, our present results showed that numerous GCIs were strongly immunoreactive for Hsc70, and to a lesser extent for Hsp70. Uryu et al. (2006) reported that they used the anti-Hsc70 and anti-Hsp70 antibodies purchased from W. Welsh. On the other hand, we selected the anti-Hsc70 antibody from Stressgen and the anti-Hsp70 antibody from Santa Cruz Biotechnology, suggesting that the different immunolabeling patterns for Hsc70 and Hsp70 in the GCIs between Uryu's results and our study may be partly due to the properties of the different antibodies.

The accumulation of insoluble -synuclein occurs widely in brains with MSA (Dickson et al., 1999; Tu et al., 1998), and -synuclein immunoreactivity is localized not only to GCIs (Gai et al., 1998; Wakabayashi et al., 1998a,b), but also to GNIs, NCIs, NNIs and dystrophic neurites (Lin et al., 2004; Wakabayashi et al., 1998a,b). In the present study, we observed the same immunolabeling patterns for neuronal and oligodendroglial inclusions between -synuclein and Hsc70, and confirmed the localization of Hsc70 immunoreactivity in GCIs, GNIs, NCIs, NNIs and dystrophic neurites. According to the previous paper (Uryu et al., 2006), co-immunoprecipitation analyses in cultured cells showed that -synuclein interacted predominantly with Hsp90 and Hsc70. Furthermore, Western blot analyses using brain homogenates from patients with -synucleinopathies and -synuclein transgenic mice revealed that Hsp90 and Hsc70 accumulated selectively in the detergent insoluble fractions. These data suggest that both Hsp90 and Hsc70 may be closely related to the formation of these neuronal and oligodendroglial inclusions through their interactions with insoluble -synuclein in brains with MSA.

LBs have been reported to be immunostained with Hsp70 (Auluck et al., 2002; Shin et al., 2005), and recent immunohistochemical studies using anti-Hsc70 and anti-Hsp70 antibodies showed that Hsc70 immunoreactivity in the LBs in nigral neuromelanin-containing neurons from patients with PD was detected more frequently than Hsp70 (Andringa et al., 2006). Our immunohistochemical studies demonstrated that similar to the LBs, Hsc70-immunopositive inclusions were observed more frequently than Hsp70 in those brains with MSA. On the other hand, our studies showed that many reactive astrocytes were intensely immunolabeled with Hsp70 in the brains with MSA, but only a few reactive astrocytes were immunopositive for Hsc70 in the same areas. These results suggest that the ligand of Hsp70 may be different from that of Hsc70, and that there may be a difference between the significance of Hsp70 and Hsc70, and Hsc70 may make a greater contribution to the formation of MSA-related neuronal and oligodendroglial inclusions than Hsp70. Moreover, Hsp70 may be induced more abundantly in reactive astrocytes than Hsc70 in the affected brain areas of patients with MSA.

The aggregation of abnormally misfolded proteins, leading to selective neuronal death, is generally thought to be a common pathological feature of neurodegenerative diseases (Agorogiannis et al., 2004). There are two major protective mechanisms against abnormally misfolded proteins: one is the molecular chaperones which regenerate the misfolded proteins, and the other is the ubiquitin–proteasome system which targets misfolded proteins for degradation and prevents their accumulation (Agorogiannis et al., 2004). GCIs are usually ubiquitinated (Kato et al., 1991; Murayama et al., 1992),

and several chaperone proteins, including B-crystallin (Kato et al., 1991; Murayama et al., 1992), 14-3-3 proteins (Kawamoto et al., 2002; Komori et al., 2003) and Hsp90 (Uryu et al., 2006), have been reported to be localized immunohistochemically to GCIs. Our present results support the immunohistochemical localization of Hsc70 and Hsp70 in GCIs. These results suggest that these two major protective systems may be operating in brains with MSA, and these molecular chaperones, including Hsc70 and Hsp70, may be overexpressed in brains with MSA to regenerate the abnormally misfolded proteins in GCIs, but that these systems may not work well in terms of protein quality control. Furthermore, the accumulation of molecular chaperones in GCIs might cause a lack of these chaperones in surviving neurons in brains with MSA, which may partially contribute to the neuronal cell death. Taken together, further research on the regulation of molecular chaperones, including Hsc70 and Hsp70, will lead to the establishment of new treatments for MSA.

4. Experimental procedures

4.1. *Tissue preparation*

We studied autopsied brains from 7 control subjects without any neurological abnormalities (age range 54–75 years, mean± SD 67.0±7.1 years) and 15 patients with MSA (age range 52–78 years, mean±SD 68.5±7.6 years). These materials were selected from the brain bank at the Neuropathology Laboratories of Kyoto University and Medical University Vienna. Among the 15 patients with MSA, 10 patients were classified as MSA-C and the other 5 patients were MSA-P, and the clinical profiles from all cases are summarized in Table 1. All brains were fixed in 10% neutral formalin for 2 weeks at room temperature. Several paraffin-embedded tissue blocks, including the basal ganglia, brainstem and cerebellum, were prepared and cut into 6- m-thick sections on a microtome. The paraffin-embedded sections were deparaffinized in xylene, followed by rehydration in a decreasing concentration of ethanol solutions. For routine pathological evaluation, the deparaffinized sections from all cases were stained with hematoxylin and eosin, Klüver–Barrera and modified Bielschowsky stains. No histological abnormalities were detected in the sections from all of the control cases, and numerous GCIs were observed in the sections from all MSA cases. The experiments were undertaken with the understanding and written consent of each subject.

Table 1 – Clinical backgrounds of all cases

Case	Age (years)/ Sex	Diagnosis	Duration of illness/ Postmortem delay
Control 1	62/M	Pancreatic carcinoma	NA/3.0 h
Control 2	68/M	Rheumatoid arthritis	NA/2.0 h
Control 3	73/M	Hepatocellular carcinoma	NA/4.5 h
Control 4	68/F	Breast cancer	NA/2.5 h
Control 5	75/M	Pulmonary emphysema	NA/2.0 h
Control 6	69/M	Lung cancer	NA/UD
Control 7	54/M	Pneumonia	NA/2.0 h
MSA 1	78/M	MSA-C	7 years/4.8 h
MSA 2	66/M	MSA-C	4 years/3.5 h
MSA 3	72/F	MSA-C	5 years/2.0 h
MSA 4	71/F	MSA-C	4 years/8.2 h
MSA 5	78/M	MSA-C	3 years/1.8 h
MSA 6	66/M	MSA-C	7 years/1.4 h
MSA 7	76/M	MSA-C	8 years/UD
MSA 8	67/F	MSA-C	2 years/UD
MSA 9	58/F	MSA-C	UD/UD
MSA 10	66/F	MSA-C	UD/UD
MSA 11	52/F	MSA-P	3 years/2.5 h
MSA 12	77/F	MSA-P	5 years/1.4 h
MSA 13	69/F	MSA-P	8 years/6.1 h
MSA 14	72/F	MSA-P	12 years/1.2 h
MSA 15	60/M	MSA-P	6 years/3.5 h

F: female; M: male; MSA: multiple system atrophy; MSA-C: MSA of the cerebellar type; MSA-P: MSA of the parkinsonian type; NA: not applicable; UD: undetermined.

4.2. *Immunohistochemistry*

To examine the immunohistochemical localization of Hsc70 and Hsp70 in normal and MSA human brains, we used a rat anti-Hsc70 monoclonal antibody (SPA-815; Stressgen, Victoria, BC, Canada, 5 g/ml) and a goat anti-Hsp70 polyclonal antibody (K-20; Santa Cruz Biotechnology, Santa Cruz, CA, USA, 2 g/ml). The deparaffinized sections were pretreated with 0.3% hydrogen peroxide (Santoku, Tokyo, Japan) in 0.1 M phosphate-buffered saline (PBS) for 30 min at room temperature to inhibit the endogenous peroxidase activity. After washing with 0.1 M PBS, the sections were blocked with 0.1 M PBS with 3% skimmed milk for 2 h at room temperature. After rinsing with 0.1 M PBS, the anti-Hsc70 or anti-Hsp70 antibody diluted in 0.1 M PBS was applied onto the sections, and the sections were incubated at room temperature overnight in a humidified chamber. After washing with 0.1 M PBS, the sections were reacted with a biotinylated anti-rat or anti-goat IgG (Vector Laboratories, Burlingame, CA, USA) diluted in 0.1 M PBS (1:200) for 1 h at room temperature, followed by an incubation with an avidin–biotin–peroxidase complex kit (Vector Laboratories) diluted in 0.1 M PBS (1:400) for 1 h at room temperature. After rinsing with 0.1 M PBS and then 0.05 M Tris–HCl (pH 7.6), the sections were developed in a colorizing solution containing 0.02% diaminobenzidine tetrahydrochloride (Dojin, Kumamoto, Japan), 0.6% ammonium nickel (II) sulfate (Wako, Osaka, Japan) and 0.005% hydrogen peroxide in 0.05 M Tris–HCl (pH 7.6) for 10 min at room temperature. As negative immunohistochemical controls, some sections were incubated with normal rat or goat serum, and no specific immunopositive staining was detected in these control sections (data not shown).

4.3. *Double immunofluorescence staining*

To compare the anatomical distribution of immunopositive GCIs containing -synuclein and Hsc70 or Hsp70, we performed double-labeling immunohistochemistry using a monoclonal mouse anti- -synuclein antibody (211; Santa Cruz Biotechnology) plus the anti-Hsc70 or anti-Hsp70